Recreating the top quark: Commissioning and monitoring of the ATLAS Inner Detector and search for New Physics with heavy particles.

Arshak Tonoyan

Dissertation for the degree of Philosophiae Doctor (PhD)

Department of Physics and Technology
University of Bergen

October 2011

Acknowledgements

While working on this thesis I have benefited from advice and support of numerous people from all over the world. I will not try to list all of them but would like to mention the ones having the biggest impact on the preparation of this work.

The first person I would like to thank is my supervisor Anna Lipniacka, who has guided me from the first day till the last hour of my PhD term. The advices I got from Anna concerning both theoretical and experimental physics as well as administrative and private matters have made significant impact on the quality of my life as a PhD student at the University of Bergen. I will never forget the hiking with Anna. Very warm gratitude goes to my co-supervisor Heidi Sandaker. Heidi introduced me to the world of detectors and was constantly helping me in all the aspects of scientific work. I am also very grateful to my another co-supervisor, Bjarne Stugu, for his practical help for all matters regarding my work. Special appreciation is addressed to Per Osland for teaching me the basics of theoretical Particle Physics and for the useful discussions on many subjects of theoretical physics.

It is hard to overestimate the input from my colleagues Alex Kastanas and Thomas Burgess whom I am gratefully acknowledging for helping me to develop the code for Inner Detector Global Monitoring and for correcting my silly mistakes in programming. I also thank my other colleagues Therese Sjursen, Øystein Djuvsland, Maren Ugland, and Trygve Buanes both for interesting and useful discussions and for helping me to get adapted for the life in Norway.

I would also like to extend my deepest gratitude to my former colleagues and advisers from the Joint Institute for Nuclear Research in Dubna, together with whom one of the papers presented in this thesis is written. Nikolai Rusakovich and Vadim Bednyakov have put the basement of my knowledge in experimental Particle Physics and helped me to get quickly involved in the top quark related analyses at the ATLAS experiment. Evgeny Khramov deserves a special appreciation not only for his great help in programming, data analysis and simulations and significant contributions both in the $t\bar{t}$ resonance and top quark charge analyses but also for the great times we have spent together in Moscow, Dubna and at CERN.

A very special thanks goes to my Armenian friends Bakur, Hovhannes, Arsen, Artem and Hayk for the fun we have had at CERN (and not only) and for the countless chats on all subjects from politics to art, from sports to programming, from business to physics, which helped me to broaden my outlook on many subjects. It would not have been possible to finish the paper about the top quark charge in time without practical help and advices from Hovhannes.

Last, but not least, I acknowledge and thank my family. I feel my parents support even at a distance of thousands of kilometers. I would like to thank my wife Goar for being so patient and for understanding and constantly supporting me throughout these

years. The quality of my life increased significantly when my little Susanna was born last year. Even though she could not help me practically, the supply of energy which I got every day from her was crucial in completing this thesis. I have already discovered my Susy.

Abstract

The ATLAS (A Toroidal Lhc ApparatuS) experiment is one of the two general purpose experiments at the Large Hadron Collider (LHC) at CERN, the European Organization for Nuclear Research. The LHC is a proton-proton and ion-ion collider built in a 27 km long circular tunnel 100 meter below the surface of the Earth. The maximum energy at which LHC is capable to collide protons is 14 TeV in the center of mass frame, but currently it is being operated at half of its maximum energy, i.e. at 7 TeV. The first collisions at the LHC took place in November 2009. Before that the LHC detectors, including ATLAS (which was already built and installed in 2007) were commissioned using muons produced from the interaction of cosmic rays with the Earth atmosphere.

The Inner Detector is one of components of ATLAS detector, which is responsible for tracking of charged particles. It consists of three independent but complementary sub-detectors, which are built using different types of charged particle detecting concepts.

This thesis is based on four papers. The first paper documents the first measurement of the top quark charge at the LHC. The analysis is done on the data collected by ATLAS in the first half of year 2011. The charge is measured with two different techniques and the results from both show that the top quark charge is in agreement with the Standard Model (SM) prediction.

The second paper is actually a book, written by collaborative efforts of almost all members of the ATLAS collaboration, describing the status of all the analyses before the launch of the LHC. I have contributed in two chapters of this book with performing simulation based analyses of the top quark charge measurement and estimating the possibility to observe supersymmetric signals with help of tau leptons.

The third paper concerns the search for physics beyond the Standard Model. Several extensions of the Standard Model predict the existence of extra gauge bosons heavy enough to decay to top-antitop pairs. The studies based on the simulation of the production of such particles with different masses are performed in order to evaluate the potential of the ATLAS detector to discover them if they exist.

The last paper summarizes the results of the commissioning of the reconstruction software for the ATLAS detector with cosmic muons and with the data from the first proton-proton collisions at the LHC. As a part of ATLAS reconstruction software, the Inner Detector Global Monitoring tool was also commissioned.

List of papers

1. **The ATLAS Collaboration, *Measurement of the top quark charge in pp collisions at $\sqrt{s}$ = 7 TeV in the ATLAS experiment*, ATLAS-CONF-2011-141, Sep. 2011.**

   The measurement of the top quark charge carried out in the lepton+jets final state in the ATLAS experiment is presented in this paper. The results were obtained using the proton-proton collision data at $\sqrt{s}$ = 7 TeV corresponding to an integrated luminosity of about 0.70 fb^{-1}. Production of the exotic quark with charge $-4/3$e is excluded at more than five standard deviations. The study is done by two methods: "jet charge" and "semileptonic B decays". I have performed the analysis with the last method.

2. **The ATLAS Collaboration, *Expected performance of the ATLAS experiment: detector, trigger and physics, chapters "Top Quark Properties", and "Measurements from Supersymmetric Events"*, CERN-OPEN-2008-020, CERN, Geneva, 2009.**

   This is a book summarizing all active analyses of the ATLAS collaboration before the LHC startup. I contributed in the two attached chapters. I estimated the possibility to measure the top quark charge with the ATLAS detector using semileptonic decays of B hadrons. The results of this work in summarized in the section 3 of chapter "Top quark properties". The other contribution I have in this book is in the chapter "Measurements from Supersymmetric Events". I have studied the possibility to determine the endpoint of di-tau distribution in mSUGRA stau co-annihilation region, called SU1 in the book. The results of the study is summarized in sub-section 5.1.

3. **E. Khramov, A. Tonoyan, V. Bednyakov and N. Rusakovich, *On the Possibility of the Search for Top–Antitop Resonances at the LHC*, Physics of Particles and Nuclei Letters, Volume 5, Number 6, 515-519, Jan. 2008**

   Another top quark related study is documented in this paper. Prospects for observation of a narrow $t\bar{t}$-resonance at the LHC are studied. Five distinct masses of the resonance are considered: 0.7, 1.0, 1.5, 2.0 and 3.0 TeV. The minimal production cross-sections needed for the observation of the Z^0-like $t\bar{t}$ resonance at the LHC are estimated for the data corresponding to 1-300 fb^{-1} of integrated luminosity. I have contributed in the simulations of the Z' boson with different masses as well as in the development of the analysis code.

4. **A. Tonoyan, M.J. Costa and J.T. Boyd on behalf of the ATLAS Collaboration, *Commissioning of the ATLAS reconstruction software with first data*, J. Phys.:**

Conf. Ser. 219 032059, 2010.

This paper is based on the poster presented by me at CHEP2009 conference. It summarizes the effort on commissioning of the ATLAS reconstruction software with cosmic muons and with first beams at the LHC. I was responsible for the commissioning of the Inner Detector Global Monitoring tool, which is a part of the ATLAS reconstruction software.

As a member of the ATLAS collaboration I am co-author of more than 80 papers.

Contents

List of Figures

Chapter 1

Introduction

The modern theory of elementary particles is the Standard Model (SM), which is based on the group of gauge symmetries SU(3)×SU(2)×U(1). So far, it successfully describes almost all the physics processes involving electroweak and strong interactions. The elementary particles in SM are divided into two groups: *fermions* and *bosons*. Bosons are responsible for mediating the interaction and they have integer spin. Fermions have spin equal to 1/2 and are the particles which feel the force. We distinguish two types of fermions: leptons and quarks, reflecting their involvement in the electroweak and strong interactions. Leptons feel only electroweak interaction, while quarks can participate also in strong interaction. The property which makes particles (quarks) to feel strong interaction is called *color*. Thus quarks are color-charged, while leptons are colorless. Fermions are grouped in three generation. Fermions from the first generation, electron (e), electron neutrino (ν_e), up quark (u) and down quark (d) constitute the ordinary matter. Members of the second generation are heavier with respect to the ones from the first generation. They are muon (μ), muon neutrino (ν_μ), charm (c) and strange (s) quarks. The third generation fermions are the heaviest ones and are named tau (τ), tau neutrino (ν_τ), top (t) and bottom (b) quarks. Two fundamental properties of fermions, mass and charge are listed in table 1.1. From the same table we can see that there exist 12 types of fermions. All fermions have antiparticles, which have the same properties except of the sign of the charge, which is opposite.

Bosons, the carriers of fundamental interactions, described by the SM are of three types. The massless photon (γ) is the only carrier of the electromagnetic force. Eight gluons (g), which carry the strong interaction are also massless. The weak interaction is mediated by three massive bosons, Z, W^+ and W^-. The mass of Z boson is measured to be 91.1876 ± 0.0021 GeV [5], while the mass of W bosons is 80.399 ± 0.023 [5]. To explain the massiveness of W and Z bosons a new particle, called Higgs boson is introduced into the Standard Model [6]. This particle has not yet been observed experimentally. The discovery of Higgs boson is one of the main goals of the LHC experiments (see section 4.2).

Although the predictions from the Standard Model are in a very good agreement with the experimental results it can not be considered to be a fundamental theory. There are two main reasons for this. The first is that the SM has 19 free parameters. These parameters are not predicted by the SM and need to be measured experimentally. The second reason is that it still does not include the theory of the gravity. In addition to these the SM has several internal problems. A good overview of these problems is

	Quarks			Leptons		
Generation	Symbol	Charge	Mass [MeV/c^2]	Symbol	Charge	Mass [MeV/c^2]
1	u	+2/3	$1.7 \div 3.1$	ν_e	0	$<2\times10^{-6}$
1	d	-1/3	$4.1 \div 5.7$	e^-	-1	0.51
2	c	+2/3	$1.29^{+0.05}_{-0.11} \times 10^3$	ν_μ	0	<0.19
2	s	-1/3	100^{+30}_{-20}	μ^-	-1	105.7
3	t	+2/3	$(173.2 \pm 0.9) \times 10^3$ [7]	ν_τ	0	<0.18
3	b	-1/3	$4.19^{+0.18}_{-0.06} \times 10^3$	τ^-	-1	1777

Table 1.1: Three generations of quarks and leptons, their charges and masses.

given in Ref. [8]. Two of them relevant to the work presented in this thesis are listed below:

- **The hierarchy problem:** The Higgs boson couples to all particles which have non-zero mass. This means that the mass of the Higgs particle depends on masses of all massive particles, when calculating it with higher order radiative corrections (loop corrections). The scale of these corrections depends on the renormalization cutoff scale Λ, which is the scale where new physics appears. Assuming that there is no new physics up to the Planck scale (10^{19} GeV), the loop corrections to Higgs mass become much larger than the predicted Higgs mass from the electroweak measurements ($\sim$100 GeV). In order to bring Higgs mass down to the electromagnetic scale careful fine-tuning need to be done, which is an unnatural procedure.

- **Dark matter problem:** The first evidence of dark matter was observed by astrophysicist Fritz Zwicky in 1933 by estimating the cluster's total mass based on the orbital velocities of galaxies in it and comparing it to it's mass estimated from the total brightness of the cluster [9], [10]. Since then several other astronomical and cosmological measurements indicate the presence of dark matter. The amount (mass) of dark matter in the Universe is estimated to be five times more than the amount of ordinary matter. The SM does not provide any dark matter candidate.

Chapter 2

Top quark physics

The top quark (t quark) is the heaviest elementary particle. It was discovered in 1995 by the CDF and D∅ collaborations at proton-antiproton collider Tevatron (Fermilab, USA) [11], [12]. Since its discovery the properties of the top quark such as production cross-section, decay channels, mass, helicity, charge are being extensively studied by the scientists working at Tevatron experiments. From the day 1 of the LHC run, the CMS and the ATLAS collaborations started to search for top quark at the LHC and by the end of 2009 they confirmed its existence [13], [14].

The decay width of the top quark predicted in the Standard Model at next-to-leading order is [15]:

$$\Gamma_t = \frac{G_F m_t^3}{8\pi\sqrt{2}}\left(1-\frac{M_W^2}{m_t^2}\right)^2\left(1+2\frac{M_W^2}{m_t^2}\right)\left[1-\frac{2\alpha_s}{3\pi}\left(\frac{2\pi^2}{3}-\frac{5}{2}\right)\right], \tag{2.1}$$

where G_F is Fermi coupling constant, m_t is the top quark mass, M_W is the mass of W boson and α_s is the strong coupling constant. With top mass ~ 172 GeV, Γ_t is equal to 1.3 GeV. The lifetime (τ_t) of the top quark is proportional to $1/\Gamma_t$ and is on the order of 0.5×10^{-24} s [5]. With this short lifetime, the top quark is expected to decay before top-flavoured hadrons or $t\bar{t}$-quarkonium bound states can form [16]. This property makes the top quark unique from the point of view of its detection techniques. Unlike the other quarks, which hadronize and are registered as jets of hadrons, the top quark can be detected via its decay products. It decays to W boson and to one of the down-type quarks (quark having charge $-1/3$). Its decay width is expected to be dominated by the channel $t \to W+b$. The other decay channels, $t \to W+s$ and $t \to W+d$ are expected to be suppressed relative to $t \to W+b$ by the square of the Cabibbo–Kobayashi–Maskawa (CKM) matrix elements $|V_{ts}|$ and $|V_{td}|$. The values of these elements and also the $|V_{tb}|$ element of the CKM matrix are estimated to be [5]:

$$|V_{td}| = 0.00347^{+0.00016}_{-0.00012}, \tag{2.2}$$

$$|V_{ts}| = 0.00347^{+0.0011}_{-0.0007}, \tag{2.3}$$

$$|V_{tb}| = 0.999152^{+0.000030}_{-0.000045}. \tag{2.4}$$

Thus, since the decay ratio of $t \to W+b$ is defined as:

$$R_{t\to W+b} = \frac{Br(t\to W+b)}{Br(t\to W+q)} = \frac{|V_{tb}|^2}{|V_{td}|^2+|V_{ts}|^2+|V_{tb}|^2}, \tag{2.5}$$

in almost 100% of cases the top quark decays to W boson and b quark.

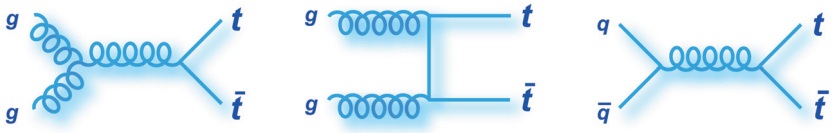

(a) (b) (c)

Figure 2.1: Feynman diagrams of $t\bar{t}$ production mechanisms at the lowest order at the LHC. In 90% of cases top-antitop pairs are produced via gluon fusion (a) and (b), while in 10% of cases the annihilation of a quark and an antiquark (c) is responsible for the $t\bar{t}$ production.

2.1 Production of top quarks

The top quark was the last quark to be discovered. The reason for this is its large mass. Before the launch of the LHC, Tevatron was the only collider able to produce top quarks. At the LHC, the main production scheme of top quarks is via gluon fusion, when two gluons interact strongly and produce a pair of top-antitop quarks ($t\bar{t}$). The $t\bar{t}$ production via quark-antiquark annihilation is less frequent, since at the LHC the particles in both beams are protons, and the only source of an antiquark in protons is sea quarks. In the Tevatron, where one of the beams consisted of antiprotons, the production was mostly via $q\bar{q}$ annihilation due to the presence of valence antiquarks in antiprotons. Figures 2.1a and 2.1b show the Feynman diagrams of gluon fusion at the lowest order, while the $q\bar{q}$ annihilation is described by the diagram in figure 2.1c.

The top quark can also be produced via weak interaction. In this case a single top or antitop quark is produced (not a pair of $t\bar{t}$). The Feynman diagrams for the weak production of single top at the lowest order are illustrated in figure 2.2. The processes described by the diagrams in the upper row of figure 2.2 are called *t-channel*. The figure 2.2d shows the single top production via *Wt channel*, while the diagram in figure 2.2e illustrates the *s-channel*.

2.2 Signatures of top-antitop pairs

Two of the analyses described in this thesis use $t\bar{t}$ production as a signal process. As discussed earlier in this chapter, the top quark decays to W boson and a b quark with almost 100% probability. Thus, decay products of a $t\bar{t}$ pair will consist of one positively charged and one negatively charged W bosons, one b quark and one $\bar{b}$ quark. The b and $\bar{b}$ quarks further hadronize producing hadronic jets, while W bosons decay either to a quark and an antiquark of different flavour or to a charged lepton and its corresponding neutrino. The Feynman diagrams illustrating all possible decay channels of a $t\bar{t}$ pair are shown in figure 2.3. Depending on the decay channel of W bosons we define three types of $t\bar{t}$ final states:

- **Dileptonic channel**, when both W bosons decay leptonically. In this case the final state consists of two jets coming from b and $\bar{b}$ quarks, two charged leptons and two neutrinos. The neutrinos can not be directly detected by ATLAS detector. But they can be detected indirectly via measuring the *missing transverse*

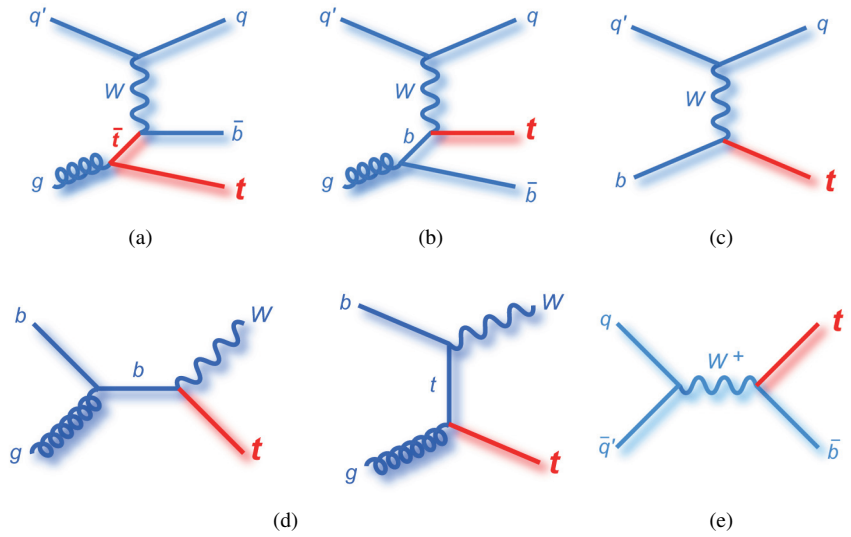

Figure 2.2: Feynman diagrams of single top $t\bar{t}$ production mechanisms at the lowest order at LHC via t-channel (a), (b) and (c), via Wt channel (d) and via s-channel (e). At hadron colliders the main contribution into single top production is coming from the t-channel.

energy, E_T^{miss}. E_T^{miss} is calculated by making use of the fact that the collisions take place along the z axis and thus the sum of transverse (to the z axis) momentum of collision products need to be 0. If by summing the momenta of all detected particles and detector noise we do not get 0 (or close to 0) we conclude that there was produced a particle (or several of them) which escaped the detector without interacting with it. The only known particles of such kind are neutrinos.

- **Lepton+jets channel**, when one of the W bosons decays leptonically, while another decays to quarks. Since these quarks also evolve into jets of hadrons, the final state in this channel includes one charged lepton, one neutrino and four jets. Two of the jets are initiated by b ($\bar{b}$) quarks. These jets can be identified by using *b-tagging* algorithms. These algorithms are based on the fact that tracks coming from decays of B mesons form a secondary vertex (displaced with respect to the collision vertex) and have relatively big impact parameter [17], [18]. This is the consequence of B meson's relatively long lifetime (1.5×10^{-12} s).

- **All-hadronic channel**, when both W bosons decay hadronically. This results in 6 jets in the final state.

Table 2.1 shows the measured values of W boson branching fractions [5]. which are used to calculate the share of each of the $t\bar{t}$ decay channels. The table 2.2 contains the results of these calculations. As can be seen from the table, the contribution of lepton+jets and all-hadronic channels is similar ($\sim 45\%$), while only in about 10% of cases the $t\bar{t}$ pair decays via dileptonic channel.

The channels containing taus are considered separately, due to the specificities of tau lepton reconstruction and identification at ATLAS [19]. Therefore, when talking

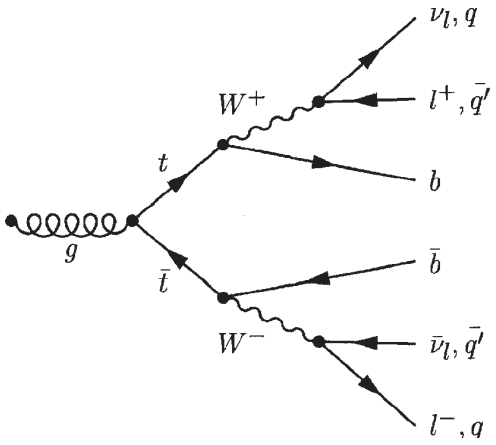

Figure 2.3: Possible decay channels of a $t\bar{t}$ pair. $\ell^{+(-)}$ refers to positively (negatively) charged lepton: electron, muon or tau.

Decay mode	Measured branching fraction, %
$W^+ \to e^+\nu_e$	10.75 ± 0.13
$W^+ \to \mu^+\nu_\mu$	10.57 ± 0.15
$W^+ \to \tau^+\nu_\tau$	11.25 ± 0.20
$W^+ \to u\bar{d}, c\bar{s}$	67.60 ± 0.27

Table 2.1: Measured branching fractions of W^+ boson [5]. Identical values are measured for the W^- boson.

about lepton+jets channel in ATLAS, we mean e+jets and μ+jets. Similarly, dilepton signature includes only ee, $e\mu$ and $\mu\mu$ channels. The pie chart in figure 2.4 shows the theoretical fractions of each of the $t\bar{t}$ decay channels.

The event display of one of the first e-μ $t\bar{t}$ dilepton candidate events with two b-tagged jets observed at ATLAS is shown in figure 2.5. The electron is shown by the green track and calorimeter cluster in the 3D view, and the muon by the long red track intersecting the muon chambers. The two b-tagged jets are shown by the purple cones, whose sizes are proportional to the jet energies.

$t\bar{t}$ pair decay channel	Fraction
$t\bar{t} \to b\bar{b}W^+W^- \to b\bar{b}(\ell^+\nu)(q\bar{q}')$	43.8 %
$t\bar{t} \to b\bar{b}W^+W^- \to b\bar{b}(q\bar{q}')(q''\bar{q}''')$	45.7 %
$t\bar{t} \to b\bar{b}W^+W^- \to b\bar{b}(\ell^+\nu)(\ell^-\bar{\nu})$	10.5 %

Table 2.2: The fractions of $t\bar{t}$ pair decay final states.

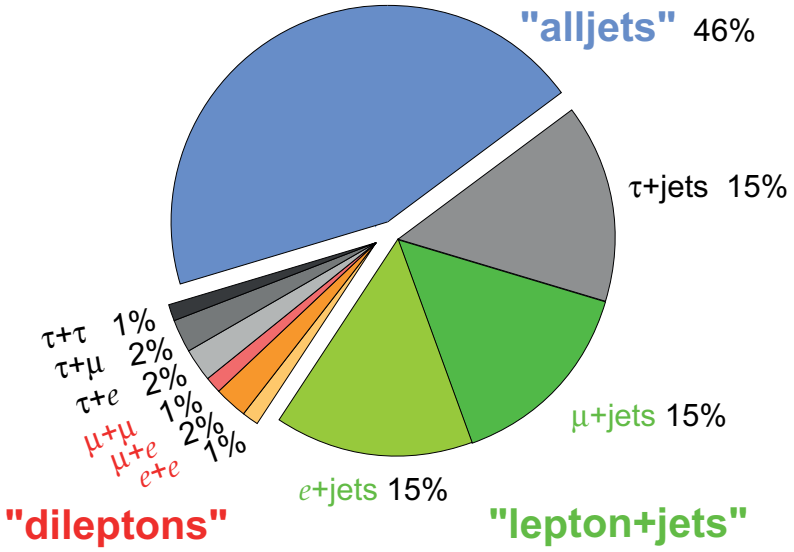

Figure 2.4: The fractions of $t\bar{t}$ decay channels.

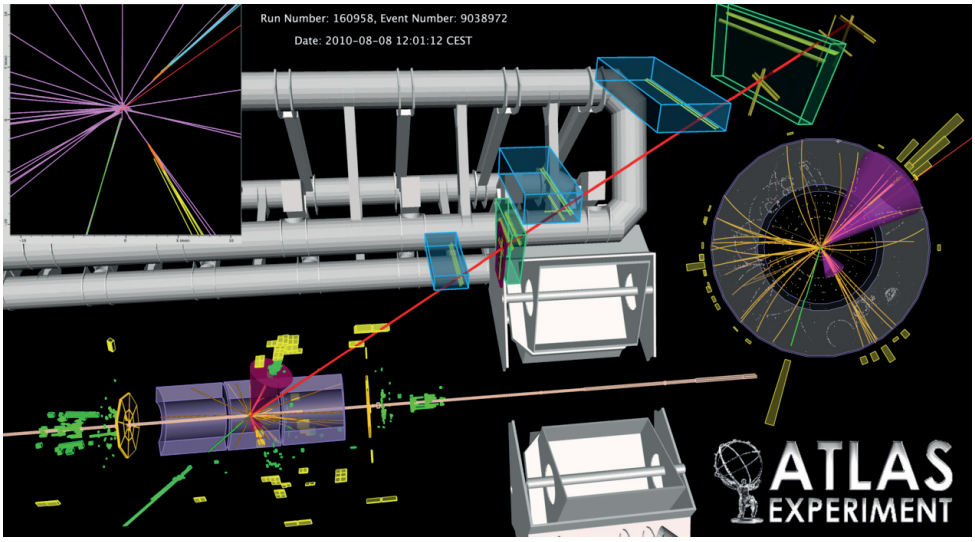

Figure 2.5: One of the first e-μ dilepton candidate events observed in ATLAS. The long red line shows the muon trajectory, while the short green line electron's trajectory. The green cluster at the end of the line shows the energy deposition by the electron in the EM calorimeter.

Chapter 3

Beyond the Standard Model physics

Though the Standard Model was tested in many experiments and has shown good agreement with their results, it is not considered to be a fundamental theory and has several unsolved problems [8]. Many extensions of Standard Model predict the existence of New Physics at the TeV scale of energies [20], at which the LHC operates.

3.1 Supersymmetry

One of the most favored extensions of the Standard Model is Supersymmetry (SUSY) [21]. It implies that all known elementary particles have super-partners in form of heavy particles with spin shifted by 1/2 with respect to the spin of their partners (ordinary particles). This means that super-partners of fermions are bosons and vise versa.

The main problem which is solved by introducing a SUSY theory is the so called *hierarchy problem* in the Standard Model, when the mass of the Higgs boson acquires quadratically divergent loop corrections. The solution comes in the form of a contribution of SUSY particles in the loop corrections, which has exactly the same size as the one from the ordinary particles, but with opposite sign. Thus the loop corrections from Standard Model particles are canceled out by their super-partners.

Another feature of SUSY is that it makes possible the existence of Grand Unified Theories (GUTs) [22], [23], which require the electromagnetic, weak and strong coupling constants to become equal at large (10^{16} GeV) scale as seen in figure 3.1. Thus all these forces can be described by one SU(5) or larger group. If the masses of SUSY particles range from $\sim$ 100 GeV up to $\sim$ 1 TeV, the run of coupling constants can be changed at this scale such that the lines intersect at one point (GUT point).

One of the main advantages of SUSY models is that many of them propose the *Lightest Supersymmetric Particle (LSP)* as a candidate for dark matter. This is the consequence of conserving the symmetry called *R-parity*, which is needed to be done to make protons stable when introducing SUSY. The *R-parity* is defined as:

$$P_R = (-1)^{2S+3B+L}, \tag{3.1}$$

where S is the spin of the particle, B is the baryon number and L is the lepton number. This definition results that all the Standard Model particles have $R = +1$, while for SUSY particles $R = -1$. In order to conserve *R-parity* the SUSY particles should be born in pairs and their decay products should contain at least one SUSY particle, which

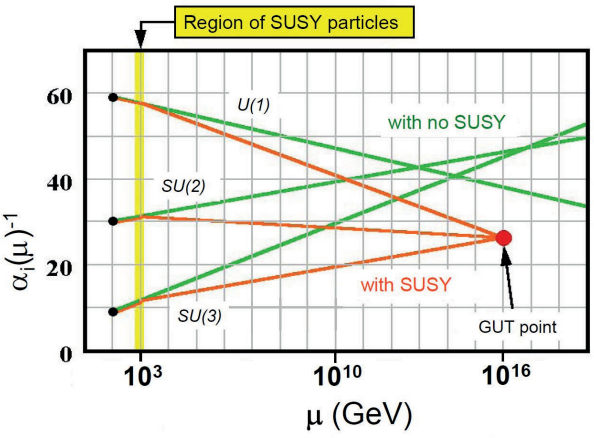

Figure 3.1: The running of all three Standard Model coupling constants without SUSY (green lines) and with SUSY (orange lines) if SUSY particles masses are $\sim$ 1 TeV [1].

implies that the *LSP* is stable. If it is also neutral and massive it becomes an ideal candidate for dark matter. Thus SUSY models can solve also one of the astrophysics problems.

The most studied SUSY model is the one with minimum number of superpartners, called Minimal Supersymmetric Standard Model (MSSM) [21]. It introduces 105 extra free parameters. The number of free parameters can be reduced by making extra assumptions. One of the widely investigated model (among MSSMs) is when SUSY breaking is gravity-mediated, whcih can be constrained by assuming the unification of forces at GUT scale. After this assumption only five free parameters remain [24], [21]. This constrained model is named minimal supergravity (mSUGRA). The mSUGRA parameters are m_0 - the scalar masses, $m_{1/2}$ - the gaugino masses, A_0 - soft breaking trilinear coupling constant, $tan\beta$ - the ratio of the vacuum expectation values of the neutral components of Higgs doublet and the sign of μ - the sign of the Higgsino mass parameter.

3.2 Heavy neutral bosons

There exist many theories of beyond the Standard Model physics that predict the existence of extra heavy neutral bosons, commonly referred to as Z'. Here we name some of the models, where the Z' can decay to top-antitop pairs. One of such models is the topcolor assisted technicolour model [25]. The technicolour models assume the existence of a new gauge interaction which generate the masses of W and Z bosons without a need to introduce the Higgs boson. In this way technicolor models solve also the hierarchy problem.

Another solution of hierarchy problem is proposed by the theories assuming the existence of extra dimensions. In these theories heavy neutral spin-2 particles are introduced, which are the excited states of massless *graviton*, the carrier of gravitational

force. The two common theories of extra dimensions are the ADD (Arkani-Hamed, Dimopoulos, Dvali) model [26], [27] and the RS (Randall, Sundrum) model [28], [29]. In the ADD model our four-dimensional world is on a brane. The extra dimensions are in form of torus with a radius r. The only force which can propagate to the higher dimensions is gravity. Thus gravity is stronger than we see on our brane. This allows to lower the Planck scale down to 1 TeV by introducing just two extra dimensions with r of the order of 0.1 mm. The more extra dimensions we require the smaller radius we need to bring the Planck scale to electroweak scale. In the RS model the Universe is a five-dimensional space with wrapped geometry. There are two branes: the "Planck" brane and the "TeV" brane. Our world with a weak gravitational force is situated on the "TeV" brane, while on the "Planck" brane the gravity is stronger.

Chapter 4

The ATLAS experiment: detector and physics

The ATLAS (A Toroidal Lhc ApparatuS) experiment is one of two general purpose experiments at the Large Hadron Collider at CERN, the European Organization for Nuclear Research. The chapter describes the detector and the physics program of the ATLAS experiment. It contains also a brief overview of the Large Hadron Collider.

4.1 The Large Hadron Collider

The Large Hadron Collider (LHC) [30] is a hadron collider designed to collide beams of protons with total energy up to 14 TeV at the center of mass frame of protons ($\sqrt{s}$ = 14 TeV). Is is also capable to collide heavy ions (*Pb-Pb*) at $\sqrt{s}$ = 2.76 TeV. The LHC is situated in a circular 27 km long tunnel buried around 50 to 175 m underground on the border of France and Switzerland. Currently, the LHC is operating at half of its maximal energy, $\sqrt{s}$ = 7 TeV. The magnets used in the LHC to steer the beams of colliding particles are made of superconducting materials (*Nb-Ti*), requiring extremely low temperatures to stay superconductors. They are cooled down to 1.9 K by a complex cryogenic system [31] using liquid helium as coolant.

The construction of the LHC started in 2001. In September 2008 the first beams were circulated in the accelerator rings. However, no collision took place till next year due to faulty electrical connections between the magnets resulting in mechanical damage and the release of helium from the cryogenic system of magnets. 53 damaged magnets were repaired and replaced. As a result of this incident, which took place 9 days after the first beam circulation, the first collisions which were initially expected to take place at the end of September 2008 were delayed and took place only at the end of November 2009. The first collisions were at injection energy, $\sqrt{s}$ = 900 GeV. The first $\sqrt{s}$ = 7 TeV collision happened in March 2010. After that the intensity of the beams was gradually increased. By September 2011 the beams contained 1.6×10^{14} protons each and were colliding with a luminosity of $\mathcal{L} = 3 \times 10^{33}$ cm^{-2}s^{-1}. The luminosity is defined such that the number of events of a particular process is given by $N = \mathcal{L} \cdot \sigma$, where σ is the cross-section of the this process. The collision rate was 20 MHz as of September 2011, but LHC is designed to be able to collide beams at up to 40 MHz frequency. The collisions take place at four points along LHC. At each of the points one of the major LHC experiments (ALICE, ATLAS, CMS and LHCb) is installed as illustrated in Figure 4.1.

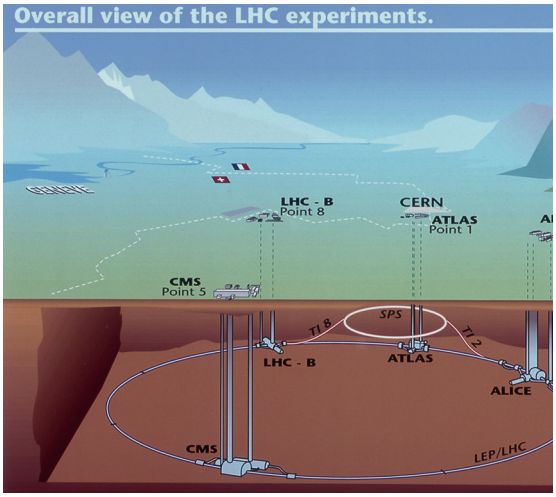

Figure 4.1: The locations of the four main LHC experiments.

4.2 Physics program

The ATLAS experiment was designed to explore the not-yet-explored frontiers of the High Energy particle physics [32]. Its design allows to both study the characteristics of already known particles and search for new particles predicted by both Standard Model (SM) and beyond SM theories. The tasks can be divided into the following groups:

- **Search for the Higgs boson**. The discovery of the Higgs boson is one of primary goals of the ATLAS experiment. The Higgs boson is the main missing piece of the SM. It is needed to describe the mechanism by which the particles obtain their masses. The experiments on the two predecessors of the LHC, the Large Electron Positron Collider (LEP) and Tevatron have performed the extensive hunt for the Higgs boson, but have not observe it. The ATLAS is able to either confirm or refute the existence of the Higgs boson in the whole range of its mass allowed by the theory. All methods of the Higgs boson search are based on the detection of its decay products. The ATLAS detector is designed to perform high precision measurements of the properties of Higgs decay products, such as electrons, muons, tau leptons, photons, quarks. The expected significance for the discovery with data corresponding to 10 fb^{-1} of integrated (by time) luminosity for different decay channels at the mass range [115; 600] is shown in figure 4.2 [2]. It can be noted that in the whole range the signal from the Higgs boson is expected to be observed by at least two standard deviation significance. The preliminary results of analyses using real data corresponding from 1.0 to 2.3 fb^{-1} of integrated luminosity are summarized in figure 4.3 [3]. The plot shows that, ATLAS can already exclude with 95% confidence the existence of Higgs boson in the mass ranges where the solid line dips below the horizontal dashed line at 1. These ranges are $(146; 232)\bigcup(256; 282)\bigcup(296; 466)$. But the Higgs particle can be hiding in the range most favoured by electroweak measurements, which indicate that it should be lighter than 148 GeV at 90% C.L [5].

- **Precision measurements of the Standard Model parameters**. Along with the Higgs searches ATLAS is designed to perform measurements of a number of SM parameters. ATLAS can measure many of these parameters with better precision than the previous experiments. The main fields where ATLAS is capable to perform precise measurements include top quark physics, W/Z boson physics and B physics.

- **Search for New Physics**. The searches for new particles predicted by the Beyond Standard Model theories (some of which are described in chapter 3) is also one of the main goals of the ATLAS experiment. The majority of the new particles in these theories decay into the known elementary particles which then can be detected. Depending on the model, the decay products can be leptons, photons, quarks, neutrinos or any combination of them. ATLAS is performing the searches for new particles by detecting their decay products.

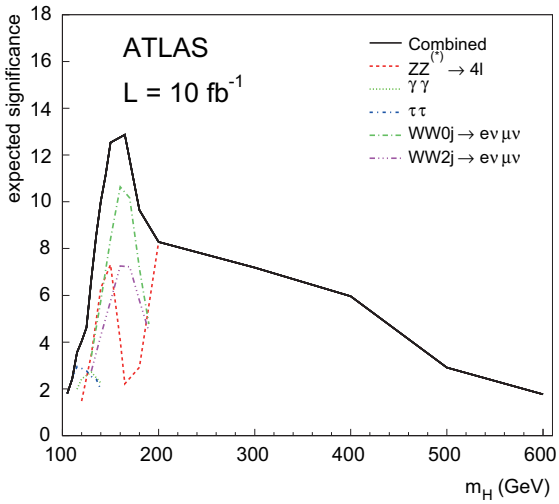

Figure 4.2: The Higgs boson discovery significance for the various decay channels and the combination with an integrated luminosity of 10 fb^{-1} for masses up to 600 GeV [2].

To perform all above mentioned tasks the ATLAS detector has to have the following components:

- High performance electromagnetic calorimeters for electron and photon identification and precise measurements of their kinematics;

- Full-coverage hadronic calorimeter with high granularity for the precise measurements of jets energy and missing transverse energy;

- Muon system capable to carry out high-precision muon momentum measurements;

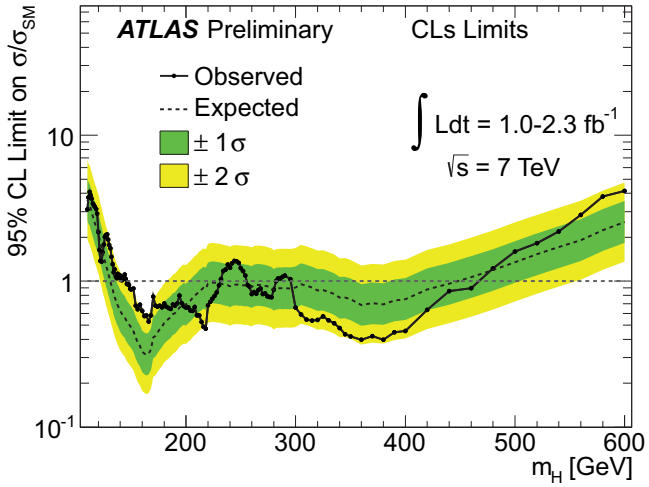

Figure 4.3: The expected and observed sensitivity of the search for the Higgs boson that arises from combining the results of searches in all decay modes studied to date. The black undulating dashed line shows ATLAS' predicted sensitivity to the Higgs boson in the mass range 115-600 GeV, based on simulations. The green and yellow bands correspond to the uncertainty in these predictions. The solid black line shows ATLAS' limit on Higgs production based on data collected up to date. ATLAS excludes with 95% confidence the existence of the Higgs boson in the mass ranges when the solid line dips below the horizontal dashed line at 1 [3].

- Efficient tracking for momentum and charge sign measurements of charged particles, reconstruction of primary (collision) and secondary (heavy flaviour and tau lepton decays) vertices;
- Fast triggering and data acquisition systems;
- The tracker and the muon system should be in a strong magnetic field in order to be able to measure track curvatures of high-momentum (up to several TeV) particles.

4.3 Overview of the ATLAS detector

The ATLAS is a multipurpose detector designed to perform searches of new physics as well as to measure the properties of already known particles and processes. The ATLAS is the largest detector among all LHC detectors. It has cylindrical shape with 25 m in diameter and 44 m in length. It consists of three main detector systems: The Inner Detector, Calorimeters and Muon System. Each of these detectors in their turn are made of several sub-detectors. Most of the ATLAS sub-detectors are divided into three parts: barrel, which is the central part of the particular sub-detector and two end-caps situated on each side of the barrel part. This division is conditioned by the orientation of detecting modules with respect to the beam (z) axis. The modules in barrel part are

oriented parallel to the beam axis, while in the end-caps the modules are placed in x-y plane. This is done to efficiently detect both particles flying at large angles with respect to the beam axis and thus crossing the sub-detectors at their central part and the ones having tracks with small θ, and passing mostly through end-caps.

ATLAS has two magnetic systems in addition to the main detector systems: Solenoid Magnet, surrounding the Inner Detector and inducing a 2 T magnetic field and three Toroid Magnets which are constructed such that the magnetic field they produce has average strength of 0.5 T and covers the area where the chambers of Muon System are situated. The cut-away view of the ATLAS detector demonstrating its size and location of its sub-detectors is illustrated in Figure 4.4. The detailed description of the ATLAS detector can be found in Ref. [33]. The features of the ATLAS detector needed to understand the work presented in this thesis are summarized in this section.

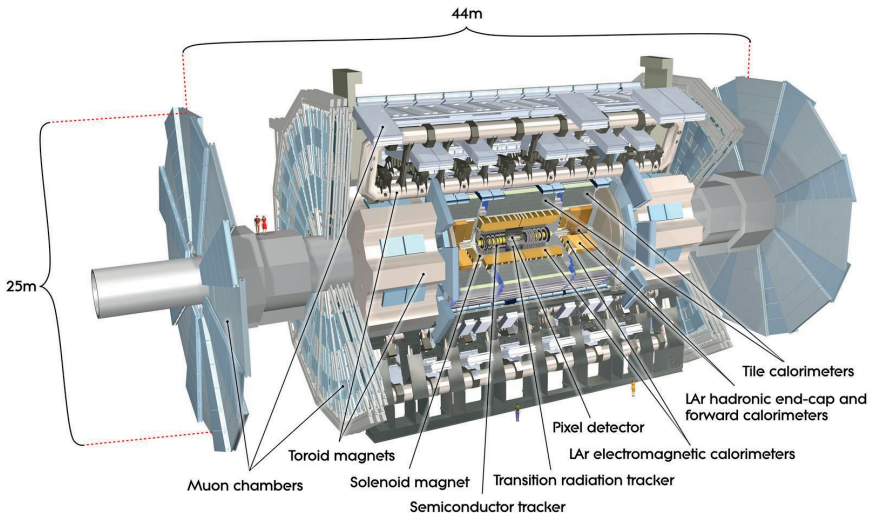

Figure 4.4: The schematic view of the ATLAS detector illustrating its size and components.

4.3.1 ATLAS coordinate system

ATLAS uses two coordinate systems: spherical and Cartesian. The ATLAS coordinate system if defined as follows:

- The origin is at the nominal interaction point.
- z-axis is along beam pipe. y points up and x points towards the center of the accelerator.
- In spherical coordinates, instead of polar angle, θ, pseudo-rapidity is used, which is defined as:

$$\eta = -ln\left(tan\frac{\theta}{2}\right). \tag{4.1}$$

4.4 The Inner Detector

Hundreds of charged particles can be produced as a result of each beam crossing creating large track density in the volume close to the interaction point. The Inner Detector (ID) is the innermost sub-detector and is responsible for detecting the tracks of charged particles. The main tasks of the ID are to measure the momentum of charged particles with high precision and to reconstruct both primary and secondary vertices with high accuracy. In order to be able to perform these tasks the ID consists of three independent but complementary sub-detectors each with high granularity of detecting elements. The cut-away view of the ID is illustrated in Figure 4.5. At inner radii, where the track density is high, high-accuracy pattern recognition requirements are met by using layers of silicon pixels (Pixel detector) and stereo pairs of silicon micro-strip layers (Semi-Conductor Tracker). At larger radii, the Transition Radiation Tracker (TRT) comprises several layers of gaseous straw tube elements interleaved with transition radiation material. With an average of 36 hits per track, it provides continuous tracking to enhance the pattern recognition and improve the momentum resolution. In addition to contributions to pattern recognition and track reconstruction TRT can provide particle identification by doing electron/pion separation over the large range of energies.

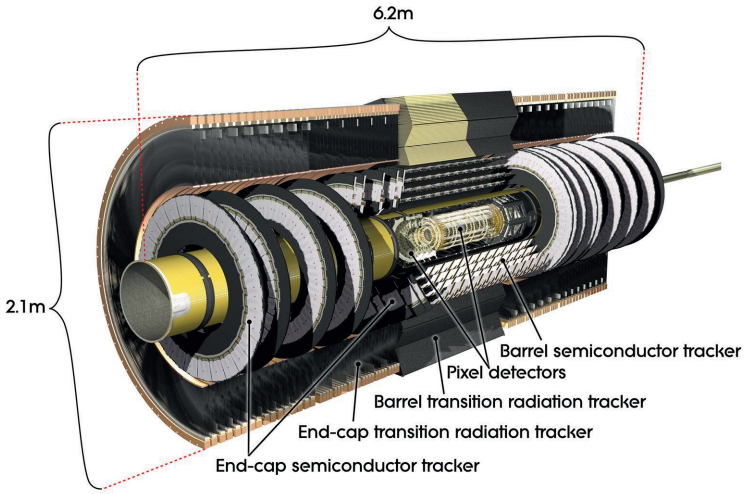

Figure 4.5: Cut-away view of the ATLAS Inner Detector.

The ID design resolutions can be parametrized with the following formula [33]:

$$\sigma(p_T) = \sigma(\infty)(1 \oplus p_T^s/p_T), \tag{4.2}$$

where $\sigma(\infty)$ is the asymptotic resolution expected at infinite momentum (intrinsic detector resolution) and p_T^s is the transverse momentum, for which the intrinsic detector resolution becomes equal to the one from the multiple-scattering. The expression (4.2) is an approximation, which works well both at high transverse momentum values, when the resolution is dominated by the intrinsic detector resolution and at low transverse momentum values, when the resolution is dominated by multiple scattering.

Track parameter	$0.25 < \|\eta\| < 0.50$		$1.50 < \|\eta\| < 1.75$	
	$\sigma(\infty)$	p_T^s (GeV)	$\sigma(\infty)$	p_T^s (GeV)
Inverse transverse momentum ($1/p_T$)	0.34 TeV^{-1}	44	0.41 TeV^{-1}	80
Azimuthal angle (ϕ)	70 μrad	39	92 μrad	49
Polar angle ($\cot\theta$)	0.7×10^{-3}	5.0	1.2×10^{-3}	10
Transverse impact parameter (d_0)	10 μm	14	12 μm	20
Longitudinal impact parameter ($z_0\times \sin\theta$)	91 μm	2.3	71 μm	3.7

Table 4.1: Expected resolution of track parameters at infinite momentum ($\sigma(\infty)$) and the transverse momentum, p_T^s, at which the multiple-scattering contribution equals that of the detector resolution [33].

The parameters $\sigma(\infty)$ and p_T^s for two pseudo-rapidity regions, one in barrel and one in end-cap, are found in table 4.1.

The tracking performance expectations from simulations are checked both with cosmic muons [34] and $\sqrt{s} = 900$ MeV and 7 TeV proton-proton collision data and are confirmed to be in good agreement with data [35], [36],[37].

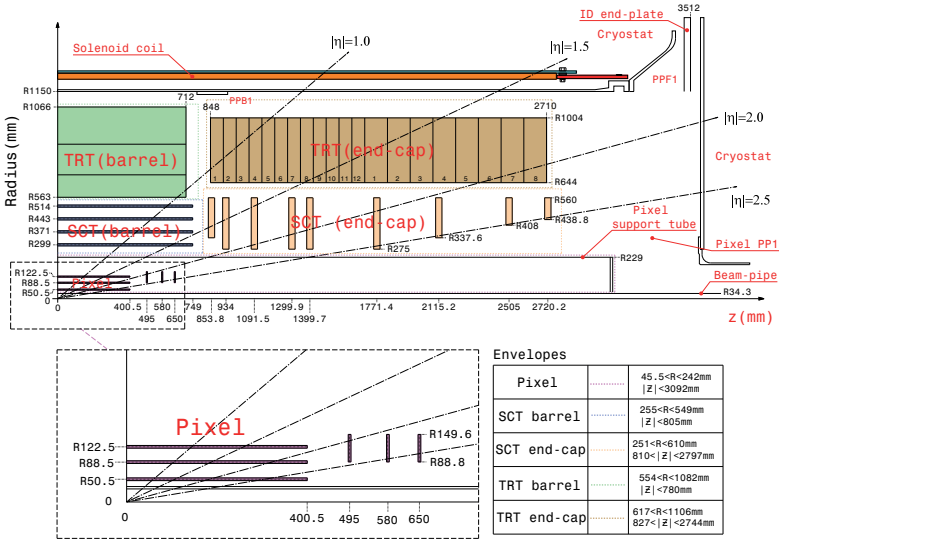

Figure 4.6: Plan view of a quarter-section of the ATLAS Inner Detector showing each of the major detector elements with its active dimensions and envelopes.

4.4.1 The Pixel detector

The Pixel detector is the closest one to the beam axis. It consists of three concentric layers of silicon pixel sensors in the central (barrel) part and three disks of sensors in each of the end-caps. The disks and layers are placed such that any particle coming from the interaction point and having a trajectory with $|\eta| < 2.5$ crosses three layers of Pixel detector (see Figure 4.6). The sensors are 250 μm thick detectors, made of

oxygenated n-type wafers with readout pixels on the n^+-implanted side of the detector. Overall 80 million sensors with size 50×400 (600) μm^2 are assembled on 1744 identical modules. Each sensor is read out by a separate electronic channel.

4.4.2 The SemiConductor Tracker

The Pixel detector is surrounded by one barrel with four layers of silicon micro-strip sensors called SemiConductor Tracker (SCT). In each of the end-caps the SCT is made in a form of nine disks placed such that silicon micro-strips are perpendicular to the beam axis. Together with three pixel disks at the end-cap part of the Pixel detector they make it possible to detect particles flying at low angles (downq to $|\eta| < 2.5$) with respect to the beam axis as shown in Figure 4.6. The SCT is made of 4088 two-sided modules. One module is composed of four silicon detectors. Each pair of these are bonded together to form 12 cm long readout strips. The pairs are glued on each side of the module at an angle of 40 μrad. The p^+-doped strips are implemented into the n-doped silicon wafer at 80 μm separation forming $p-n$ configuration. There are 768 active strips per sensor, plus two strips at bias potential to define the sensor edge. Thus SCT has approximately 6.3 million readout channels. The intrinsic resolution per module is 17 μm in r-ϕ plane and 580 μm in z direction.

4.4.3 The Transition Radiation Tracker

The third and outermost sub-detector of the ID is the Transition Radiation Tracker (TRT) consisting of 73 planes of 4 mm diameter straw tubes in the barrel part and 160 planes in each of the end-caps, thus providing large number of hits (in average 36) per track. The tubes are filled with gas mixture in following proportions: 70% Xe, 27% CO_2 and 3% O_2 [38]. In the barrel region, where the straws are parallel to the beam axis there are 52 544 straws with length of 144 cm. Each end of the straw is read out by a separate channel. In the end-caps region, the 37 cm long straws are arranged radially in wheels making them perpendicular to the beam axis. These straws are read out only from one end. The total number of straws in both end-caps is 245 760. End-caps and barrel together provide approximately 351 000 read-out channels [38]. The TRT covers the pseudo-rapidity range of $|\eta| < 2$ (Figure 4.6). Its intrinsic resolution in r-ϕ plane is 0.13 mm per straw. TRT does not provide measurement of the z coordinate.

4.5 Calorimeters

All calorimeters in ATLAS, except of the Forward Calorimeter, are sampling calorimeters made by alternating of layers of active medium and absorbers. They provide good containment for electromagnetic and hadronic showers, and also limit hadron punch-through into the muon system. The total thickness of the calorimeters at $\eta = 0$ is 11λ (interaction length). This has shown to be sufficient to reduce the punch-through into the muon system to an acceptable level. All calorimeters together cover the $|\eta| < 4.9$ range. The components of the ATLAS calorimeter system are illustrated in figure 4.7.

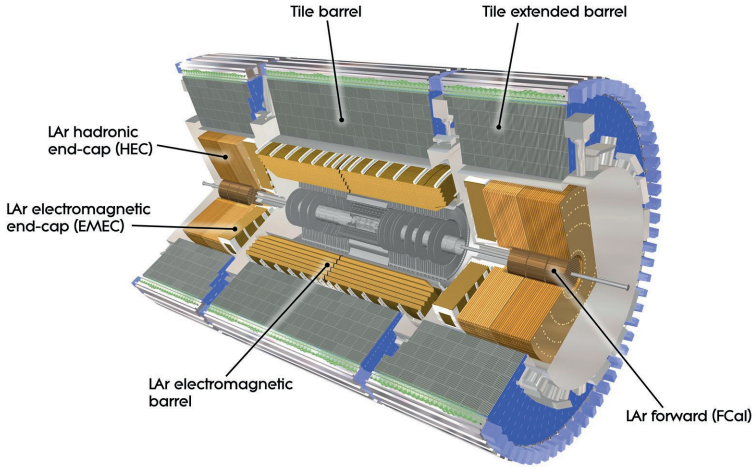

Figure 4.7: Cut-away view of ATLAS calorimeters.

4.5.1 The Electromagnetic calorimeter

The Electromagnetic (EM) Calorimeter is surrounding the Inner Detector and is a liquid argon (LAr) detector with accordion-shaped electrodes and lead absorber plates over its full coverage. The electrodes are made of three layers of copper interlayed with kapton. The two outer layers are under high voltage, while the middle one is used for read out of the signal. The gaps between absorbers and electrodes are filled with liquid argon, which is the active material of the detector. The accordion geometry provides complete ϕ symmetry without azimuthal cracks.

When an electron or a photon passes through the calorimeter, it initiates an electromagnetic shower when interacting with the lead absorbers. The components of the shower, then ionize the LAr, and the current produced by the drift of the ionization products towards electrodes is read out as signal. The EM calorimeter is divided into barrel part ($|\eta| < 1.475$) and two end-caps ($1.375 < |\eta| < 3.2$). The barrel part has a cylindrical shape with inner diameter of 2.8 m and outer diameter of 4 m. The length of the cylinder is 6.4 m. The end-caps have a wheel-shape. They are 0.63 m thick and with inner diameter of 0.66 m and external diameter of 4.2 m. In the precision measurement region which is defined as $|\eta| < 2.5$ the EM consists of three layers in depth. The rest of the EM is segmented into two layers. The granularity of samplings are η and layer dependent and are from 0.025×0.25 to 0.1×0.1 in the η-ϕ plane. In the region ($|\eta| < 1.8$) the EM calorimeter is complemented by presamplers consisting of a LAr layer of thickness of 1.1 cm (0.5 cm) in the barrel (end-cap) region in order to pick up the showers which started before the particle reached the EM calorimeter.

4.5.2 The Hadronic Tile calorimeter

The Hadronic Tile Calorimeter (TileCal) is placed behind the EM calorimeter and covers the range $|\eta| < 1.7$. It has a cylindrical shape with internal and external radii of 2.28

m and 4.25 m respectively. The total length is 11 m. It is made of 14 mm thick layers of iron absorbers interlayed with 3 mm thick scintillating tiles. When interacting with iron, a hadron produces a hadronic shower. The signal from the components of the shower is then collected by the scintillators. The total thickness of the TileCal is 2 m, which corresponds to 8 λ (interaction length). It is segmented in three layers in depth. The granularity of samplings in the first two layers are 0.1×0.1, while the last layer has coarser samplings with 0.2×0.1 size in the η-ϕ plane.

4.5.3 The Hadronic End-cap calorimeter

The Hadronic End-cap calorimeter (HEC) consists of two wheel-shaped parts, each placed at one of the two ends of the EM calorimeter. Its covers $1.5 < |\eta| < 3.2$ range. The HEC uses the same detecting technology as the EM calorimeter, but with flat absorbers made of copper. The first 24 plates of absorbers (counted from the side closer to the EM calorimeter) have 25 mm thickness, while the remaining 16 are two times thicker. The size of the readout cells is $\Delta\eta \times \Delta\phi = 0.1\times0.1$ in the region $|\eta| < 2.5$ and 0.2×0.2 for larger values of η.

4.5.4 The Forward calorimeter

The purpose of the Forward Calorimeter (FCAL) is to measure both electromagnetic and hadronic showers at high eta region. Its coverage is $3.1 < |\eta| < 4.9$. The FCAL has LAr as a sensitive medium, but uses different detecting technology. It consists of three modules in each end-cap. The first module is intended to register the electromagnetic shower, while the second and third module is designed to catch the hadronic shower. All modules are made of copper plates placed next to each other. The plates of the first module have 12260 holes in them, in which the electrodes are placed. An electrode consist of a copper-made rod placed into a copper-made tube. The gap between the rod and the tube is filled with LAr. The second and third modules have 10200 and 8224 electrodes respectively. The electrods in these modules consist of tungsten rods placed into copper tubes.

4.6 The Muon spectrometer

The outermost sub-detector of the ATLAS is the Muon spectrometer (figure 4.8). It triggers muons and provides precision measurements of the their track parameters. The Muon spectrometer is situated in a magnetic field with average strength of 0.5 T, generated by air-core toroidal magnets. The magnets are configured such that the field they produce is orthogonal to the trajectories of the muons coming from the interaction point. The muon system uses four different types of detecting technologies: Monitored Drift Tubes (MDT), Resistive Plate Chambers (RPC), Thin Gap Chambers (TGC) and Cathode-Strip Chambers (CSC). The MDTs and the CSCs are used to measure the track curvature with high precision, while the RPCs and TGCs are primarily aimed for triggering purposes.

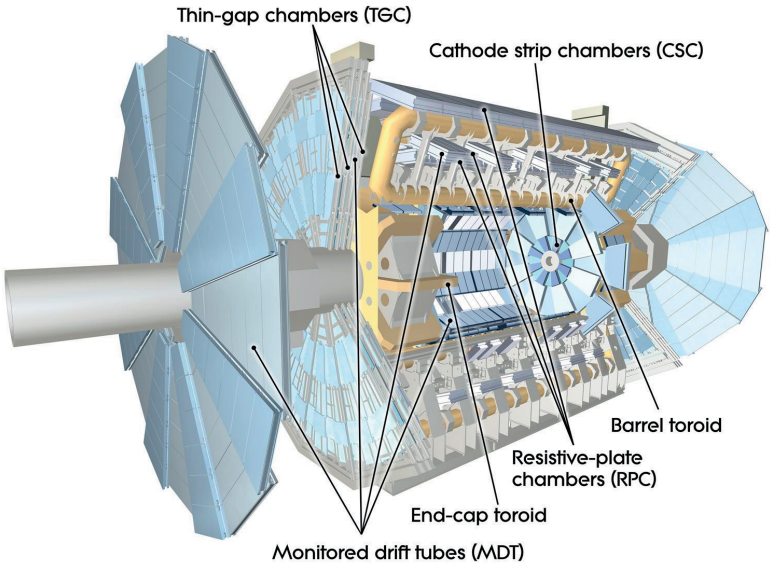

Figure 4.8: Cut-away view of ATLAS Muon spectrometer.

4.6.1 Monitored Drift Tubes

The MDT is the main technology for the precision measurements of muon track parameters at ATLAS. The muon passing through the ATLAS detector in the range of $|\eta|$ < 2.7 can cross three to eight layers of MDTs. The MDTs are drift tubes filled with Ar/CO_2 (93%/7%) gas mixture under 3 bar pressure. The tubes are aluminum made with 30 mm in diameter and are concentric around a tungsten-rhenium 50 μm thick wire. Muons crossing an MDT ionize the gas and the electrons are collected by the wire which is at 3080 V potential with respect to the tube walls.

4.6.2 Cathode-Strip Chambers

The particle flux at the first layer in the region $|\eta| > 2.0$ is above the threshold at which MDT can provide efficient counting. Therefore the first layer of muon system in the range $2.0 < |\eta| < 2.7$ consists of cathode-strip chambers, which are multiwire proportional chambers. The strips of the cathodes on one side is parallel to the wire while on the other side it is perpendicular. The position of the muon trajectory intersection is defined by interpolation between the charges induced on neighbouring strips. The wires are 30 μm thick. The operation voltage is 1900 V.

4.6.3 Resistive Plate Chambers

The RPCs have a threefold purpose. They provide bunch-crossing identification (BCID), discriminate based on the muon transverse momentum and provide a complementary measurement of the muon coordinate which can be used for pattern recognition and muon track reconstruction. RPCs cover only the barrel region $|\eta| < 1.05$. They are

gaseous parallel electrode-plate detectors. The electric field between the plates is 4.9 kV/mm. The signal is read out through capacitive coupling to metallic strips mounted on the plates.

4.6.4 Thin Gap Chambers

The TGCs were selected to perform triggering in end-cap region $1.05 < |\eta| < 2.4$. They, like RPCs, can also provide the measurement of the ϕ coordinate to complement the measurements of the MDTs in the bending direction. The TGCs are multi-wire proportional chambers with small space between wires and the cathode and large space between the wires.

4.7 Magnets

In order to measure the momentum of charged particle a complex system of superconducting magnets is employed by ATLAS. It consists of two parts. The first part is a 5.8 m long solenoid surrounding the Inner Detector with diameter of 2.5 m. It generates a 2 T axial field at the center and 2.6 T at the windings. The field of this magnet is used to measure the momentum of charged particles in the Inner Detector. The second part consists of three air-core toroid magnets, each made of eight coils. Each of these coils is placed in a separate cryostat. The goal of toroid magnets is to bend trajectories of muons in Muon Spectrometer. In the range $|\eta| < 1.4$, the bending is provided by the large barrel toroid. The two smaller end-cap toroids cover the range of $1.6 < |\eta| < 2.7$, while in the range of $1.4 < |\eta| < 1.6$, the field is generated both by the barrel and end-cap magnets. The outer size of the magnet system is 22 m in diameter and 26 m in length. The operational temperature of all magnets is 4.5 K.

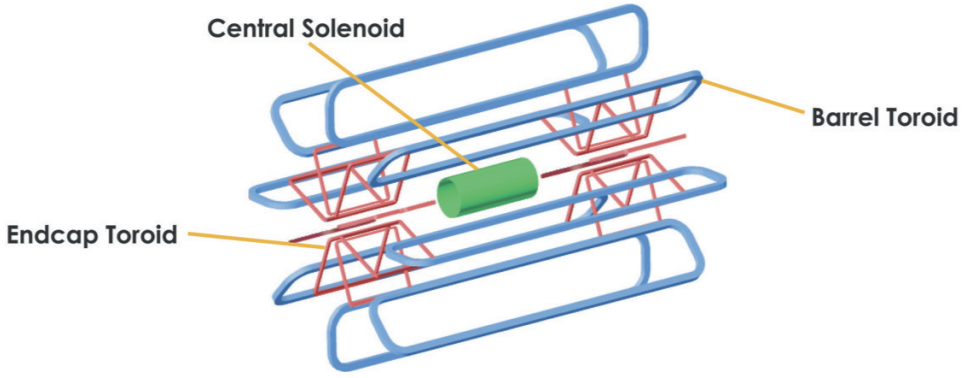

Figure 4.9: The geometry of ATLAS magnet system.

4.8 Trigger

As mentioned in section 4.1, the design frequency of collisions at the LHC is 40 MHz. It is not possible to record events at this high frequency from all $\sim 10^8$ read-out channels of the ATLAS detector. Therefore a trigger system is needed to reduce the 40 MHz input rate to an output rate of about 200 Hz for recording and offline processing. This limit is conditioned by the average data rate of $\sim$ 300 MB/s, determined by the computing resources for data storage and processing. The ATLAS trigger chain has three levels. The level 1 (L1) trigger uses data from the the calorimeters and muon system to decide weather event looks interesting or not. The output rate of L1 can be up to 75 kHz. L1 is a hardware based trigger. The level 2 (L2) as well as level 3 (Event Filter, EF) are software based triggers. They can use the data from all sub-detectors, but L2 reconstructs the data only from the Regions of Interests (RoI) determined by the L1 trigger. At the input of the Event Filter the data rate is already reduced to 3 kHz. In its turn the EF reconstruct the full event and based on the predefined signatures selects events to be recorded. The signatures depend on the goal of a particular run and are based on combinations of reconstructed physics objects, i.e. electrons, muons, jets, taus, photons or transverse missing energy. There are also signatures when the trigger is fired if cosmic muon passes through the detector or if inelastic collisions take place. The schematic view of ATLAS trigger system can be seen in figure 4.10.

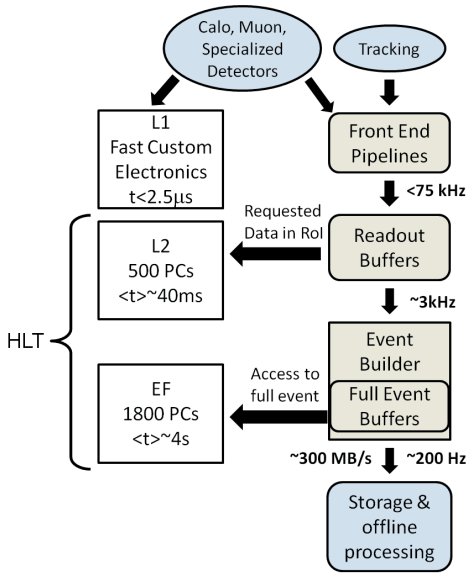

Figure 4.10: The schematic view of ATLAS trigger chain.

4.9 Data and simulation processing skim

When a trigger is fired the signals from the whole detector is read out. These signals come from a single event: either bunch crossing or passage of cosmic muon through

the detector. They are digitized and saved in a format called Raw Data Objects (RDO). Then, the reconstruction procedure is performed which converts the digitized signals from the detector into objects and stores the events in ESD (Event Summary Data) format. The ESD has an object-oriented representation. Physics analysis can already be performed using ESD files, but the event size in these files is big since the event contains the information from all the channels of the detector. Therefore ESD is not suitable for physics analysis. A reduced event representation, derived from ESD and called Analysis Object Data (AOD) is more suited for analysis. It contains physics objects and other elements of analysis interest. To even more reduce the size of an event, the Derived Physics Data (DPD) is introduced. It is an ntuple-style representation of event data and can be directly used by the analysis tool ROOT [39], widely used in High Energy experiments. Events in DPD files contain objects intended to be used by a particular type of analysis. RDO, ESD and AOD files are produced centrally, while DPDs are produced either by working groups or by individual users.

The simulation of physics processes at the ATLAS detector are performed in several steps. The first step is the event generation, which is the simulation of production and decay of particles. This is done by using one of C++ or Fortran based event generators. Pythia [40] and Herwig [41] are among the most widely used event generators in Particle Physics. The next step is the simulation of interaction of generated particles with the ATLAS detector. This is done by using GEANT4 simulation toolkit [42] intended to simulate the physics processes of particles interaction with matter. The third step is so called digitization, which is the simulation ot detector response. After this step the simulated data has the same format as the real data coming from the detector, i.e. RDO format. Thus the reconstruction and further steps on simulated data are done in the same way and with help of the same software as for real data.

All the procedures described above are carried out within the ATLAS software framework, Athena [43].

Chapter 5

The Inner Detector Global Monitoring

The Inner Detector Global Monitoring (ID Global Monitoring) is a tool which is responsible for monitoring how the ATLAS Inner Detector (ID) works as a tracker. Combined ID tracks, made of hits from all three sub-detectors are used as the primary tool. In addition to combined tracks, track segments made by hits from a single sub-detector are used. Besides tracks, the occupancy of the ID, ID hit timing information and bunch crossing and level 1 trigger identifiers (BCID and L1ID respectively) are used to monitor the stability and the synchronization of ID sub-detectors. The aim is to determine both the status of the detectors and the impact which the sub-detector issues have on the tracking performance of the ID. The ID Global Monitoring was launched in 2005, when the ID, being still on the surface, took its first cosmic muons data. Since then it has been continuously developed and commissioned first with cosmic muons and later with $\sqrt{s} = 900$ GeV and $\sqrt{s} = 7$ TeV proton-proton collisions. The ID Global Monitoring is part of the ATLAS Data Quality Monitoring (DQM). It produces and analyzes over 250 histograms both in online mode, when a quick feedback is required and in offline mode, when more detailed analysis is provided. The results shown here are based on the cosmic muons runs taken from September 2008 till March 2009 and proton-proton collision runs taken from October 2009 till March 2010. An event with a cosmic muon passing through the Inner Detector is shown in figure 5.1.

5.1 Software Design and Tools

From the software point of view the ID Global Monitoring is one of the packages of ATLAS reconstruction software. It is a C++ based package and consists of several different tools. When each tool is called it produces a set of ROOT [39] histograms based on the data. The core functionality for this is provided by the `ManagedMonitoringToolBase` Athena package from which ID Global Monitoring inherits. A basic set of functions is implemented in this package to store histograms in the Athena Histogramming service, to save and to retrieve the monitoring related information.

Figure 5.2 shows the structure of the ID Global Monitoring package and its class inheritance. In the center is the `InDetGlobalMotherMonTool`, the base class of all tools, providing some basic functionality for the monitoring. This is an extension of the functions provided by `ManagedMonitoringToolBase` that is common to all monitoring tools. For tools requiring trigger awareness the class `InDetGlobalMotherTrigMonTool`

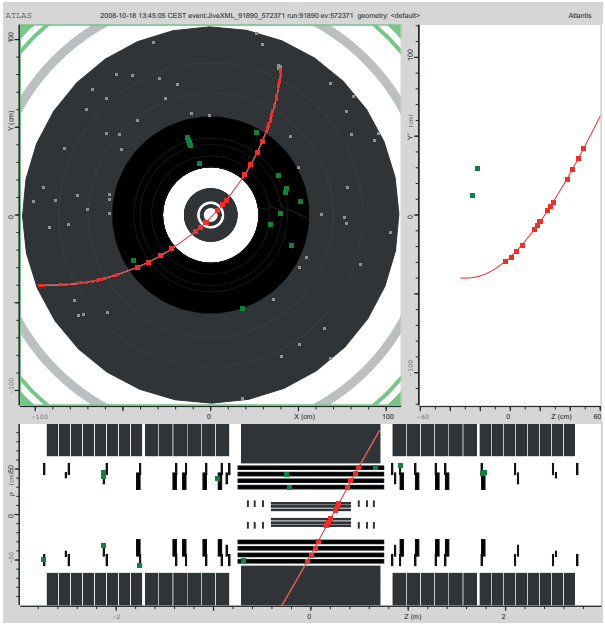

Figure 5.1: An event display showing the x-y (top left), z-ρ (bottom) and z-y (top right) projections of the track of a cosmic muon passing through the Inner Detector. The track is shown by a red line. The hits associated to the track are shown by red squares.

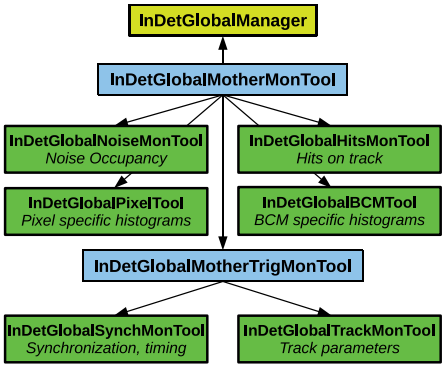

Figure 5.2: The class structure of ID Global monitor. The blue boxes are the base classes of all the tools. The boxes in green are tools called by the monitor to produce the Data Quality histograms. The manager is in yellow.

extends to cover these too. All tools inherit from one of these classes. In addition these, one monitoring manager, the `InDetGlobalManager`, is set up to control the execution of each tool and to set common options. In order to save CPU overhead the manager also retrieves the data collections used by the monitoring tools.

The ID Global monitoring runs as a part of the ATLAS reconstruction chain. This means that after reconstruction is finished the monitoring runs on the data produced by reconstruction. The package relies on both tracking information and information on raw hits in the detector. It runs both at the data taking stage (onine) and at the bulk data reconstruction stage (offline). The code is the same for these two modes, but the infrastructure to run it differs. During online running the checks are primarily intended to spot problems as they arise and give quick feedback to detector operation team. The online plots are checked by the General Online Data Quality (DQ) shifter and can assist the online DQ shifters of the ID sub-detectors. In online running mode the events are sampled after the level 1 trigger and only a fraction of all recorded events are passed through the monitoring tools. The main limiting factor for the sampling rate is the number of monitoring applications running in parallel, which is limited by CPU capacity. When the monitoring is enabled in the offline reconstruction stage the full run is checked and the output is made for each trigger stream, making it possible to have the checks on exactly the data that will be used for physics analyses.

5.2 Monitored Objects and Quantities

5.2.1 Tracks

Tracks are very sensitive to problems which may occur during the operation and reconstruction of the data from the ID. They are the final reconstructed ID objects and thus they carry information about the ID as a single tracker. Looking at the distribution of track parameters, number of hits and track quality variables it is possible to get indications about misalignment, inefficient or noisy modules, wrong magnetic field

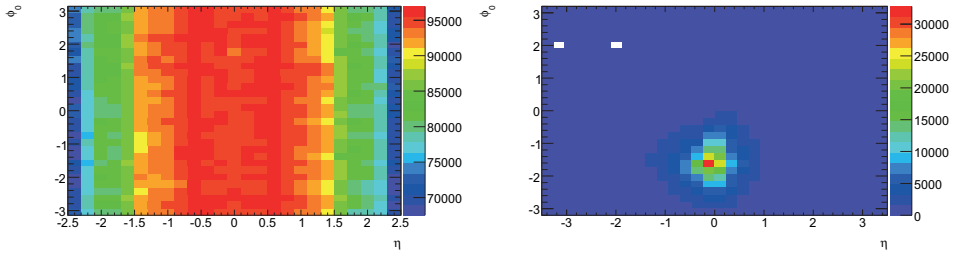

(a) (b)

Figure 5.3: Examples of 2D histograms showing distributions of ϕ_0 versus η of tracks in proton-proton collision run number 155112 (a) and in cosmic muon run 121513 (b). They show how the distribution looks like when the ID sub-detectors and tracking algorithm are performing as expected.

map or problems in track reconstruction algorithms. Tracks are the main tool of the ID Global monitoring. All available ID track collections are used by the ID Global monitoring. The following parameters of combined tracks made of both from TRT and Silicon (Pixel + SCT) hits are monitored: azimuthal angle ϕ_0, pseudo-rapidity η, longitudinal and transverse impact parameters z_0 and d_0 and charge over momentum q/p. Besides the track parameters, the track multiplicities (number of tracks per event) and the χ^2/Ndf of track fit are also monitored. Each of the monitored quantities are stored in one-dimensional (1D) histograms. The track parameters as well as track multiplicities and rates are monitored not only per run, but also for smaller time periods called Luminosity Blocks (LBs). One LB contains roughly 2 minutes of data taking, but this can vary due to run conditions and other operational issues. This kind of plots help to check if the monitored quantities are stable during the run.

In addition to 1D histograms, several 2D histograms are filled with the different combinations of track parameters, like ϕ_0 vs η or d_0 vs ϕ_0. Figure 5.3a shows the ϕ_0 vs η distribution in case of a collision run. The distribution is expected to be homogeneous in ϕ_0 and symmetric in η with respect to $\eta = 0$. Holes and asymmetries in this distribution may indicate regions where the tracking is not as efficient as expected. The distribution of the same parameters for cosmic muon runs are completely different as seen on figure 5.3b. As most of the tracks in this plot are tracks from the cosmic muons, and the muons are coming straightly from the open shaft above ATLAS, they have ϕ_0 equal to $\pi/2$ and η close to 0. Both plots illustrate runs where the ID and tracking reconstruction algorithms worked as expected.

5.2.2 Hits on tracks

To further check the properties of tracks, the hits associated with a track are considered. This is done by monitoring the number of hits on track in every sub-detector (Pixel, SCT and TRT). An example histogram for this check is shown in figure 5.4. As can be seen from the figure, most tracks have 11 Silicon hits (8 SCT + 3 Pixel), and 30-35 TRT hits. Another important goal is to find areas with malfunctioning detector parts or inefficient tracking. This is done by both looking at average number of hits on tracks

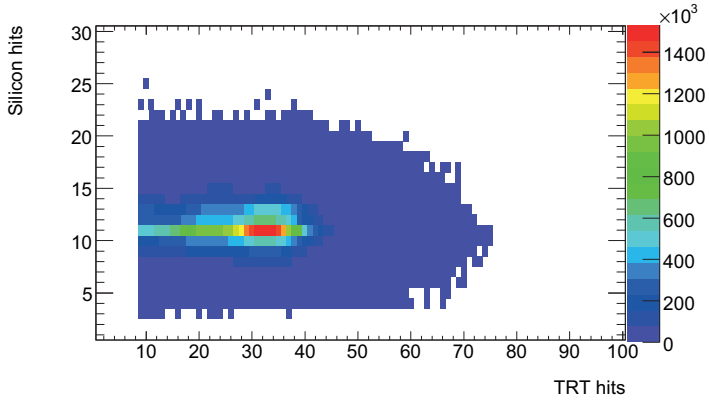

Figure 5.4: Number of Silicon hits on track versus number of TRT hits on track, showing the expected distribution of hits when the tracking is efficient.

by ϕ_0 or η of tracks as well as with help of 2D histograms showing one of coordinates of the hits versus other. Figure 5.5 illustrates the number of hits versus spatial X and Y coordinates in runs 155112 (5.5a) and 141561 (5.5b). Run 155112 has the typical distribution of the hits when the full ID is operational and tracking performs well. In run 141561 only TRT was operational and the TRT tracking algorithm had a problem in the code which made it unable to reconstruct tracks crossing the x-axis at its negative side. As can be seen from the figure, the number of hits at the negative side of the x-axis is smaller than in other regions of the detector.

5.2.3 Noise occupancy

One of the main parameters monitored by individual sub-detector monitoring systems is the noise of the detecting units (pixels, strips, straws). For correct track reconstruction it is important to ensure that the noise is as low as possible and that noisy detecting elements are known and taken into account. Unlike the individual sub-detector monitoring systems, the ID Global monitoring does not monitor the noise of a single detecting element, but it monitors the noise occupancy of the particular whole sub-detector. Noise occupancy is defined as number of hits not associated with tracks divided to the number of all detecting channels. This definition was initially chosen for cosmic data taking mode. As these hits are not necessarily introduced by noisy detector elements but can also originate from particles whose tracks were not reconstructed, this definition does not always represent the noise originating from electronics. This is especially true for collision data taking mode when the particle multiplicity is high. Thus the Noise occupancy tool monitors a quantity which has contributions both from the electronic noise and from the tracking algorithm inefficiency. The Noise occupancy tool is made to mostly serve for online purpose, when a shifter can follow the stability of the noise occupancy during the run looking at the noise occupancy plotted for last sampled 2000 events.

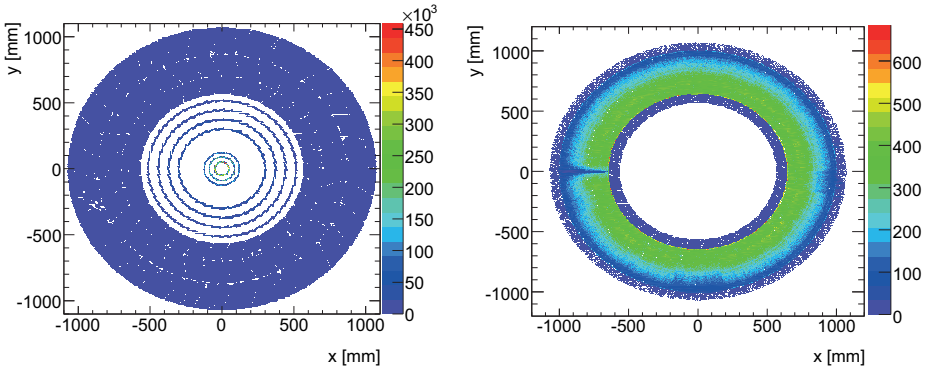

Figure 5.5: Hit map of the ID barrel hits on track in x-y plane of runs 155112 (a) and 141561 (b). In the run 155112 all the ID sub-detectors were operational and the tracking algorithms performed well. All 3 layers of Pixel detector and all 4 layers of SCT are seen and the hits are equally distributed in them. Only TRT was operational in the run 141561 and the TRT tracking algorithm had a problem in the code, which made it inefficient in the reconstruction of the tracks crossing the x-axis at its negative side.

5.2.4 Synchronization

One of the main goals of the ID Global Monitoring is to ensure that the ID is synchronized with the LHC clock and ATLAS Level 1 trigger and that the sub-detectors of the ID are working synchronized against each other. The quantities used for this purpose are bunch crossing identifier (BCID) and level 1 trigger identifiers (L1ID). Both these identifiers are cyclic. They go from 0 to 3563 and correspond to each possible crossings of bunches at the LHC. All read-out drivers (ROD) use these identifiers to ensure that the signals collected from the detecting moduls belong to the same event. It is expected that the hit occupancy is significantly higher for the BCIDs corresponding the paired colliding bunches than for the ones corresponding to empty bunches. Figure 5.6a shows the average number of hits in Pixel detector as function of BCID. In this run the bunches having BCID 1, 201 and 401 are paired (there are 2 bunches with the same BCID circulating in the LHC in opposite directions) and colliding. Thus the average number of Pixel hits for events corresponding these BCIDs are more than 650. In addition to paired bunches, there are 6 unpaired bunches in this run, which do not collide with other bunches, but they circulate through ATLAS and interact with collimators. While these bunches do not collide, the number of Pixel hits for these BCIDs is still high enough (200-300) to be distinguished from the noise, which in average gives 4-5 Pixel hits per event. Figure 5.6b shows that significant amount of ID tracks are reconstructed only in the case of colliding bunches. This is expected despite the high occupancy of Pixel detector, since the particles produced from the interaction of unpaired beams with collimators move almost horizontally and do not pass through the other ID sub-detectors (SCT and TRT) and thus do not satisfy the tracking algorithm requirements.

The BCID and L1ID taken from the RODs of the ID sub-detectors are checked

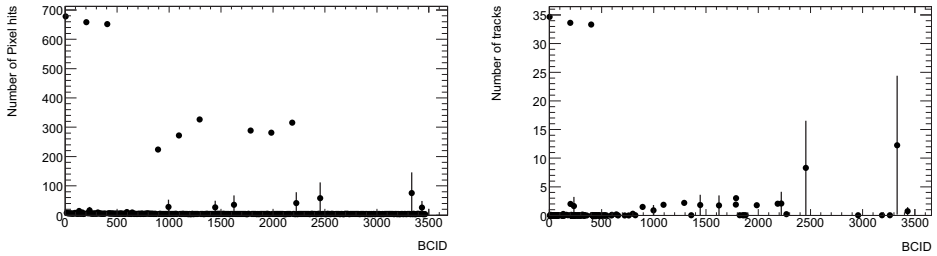

(a) (b)

Figure 5.6: a) Example plot showing the average number of Pixel hits as a function of BCID. The three points with high number of hits (600-700) correspond to the colliding bunches. The six points where number of hits is 200-300 correspond to non-colliding bunches. They are clearly distinguishable from the colliding ones. b) Example plot showing the average number of the ID tracks as a function of BCID. Colliding bunches produce in average 33-35 tracks, while number of tracks corresponding to BCIDs of unpaired or empty bunches usually does not exceed 5. The ones which exceed are single events (see the size of the error) when a cosmic muon passed through the detector.

against each other to verify if all RODs are correctly timed. If a timing mismatched is observed it is logged in a histogram as in the case of the run 155122 (figure 5.7a), when during 35 events some of TRT RODs were having different BCIDs than their neighbor RODs. To trace exactly which RODs were mismatched, one can use the histogram shown in figure 5.7b. It shows that the RODs number 31-33 and 35 are mismatched with their neighbors.

5.3 Data Quality Checks

Plots produced by the monitoring packages are checked automatically via the Data Quality Monitoring Framework (DQMF) [44]. This framework performs automated

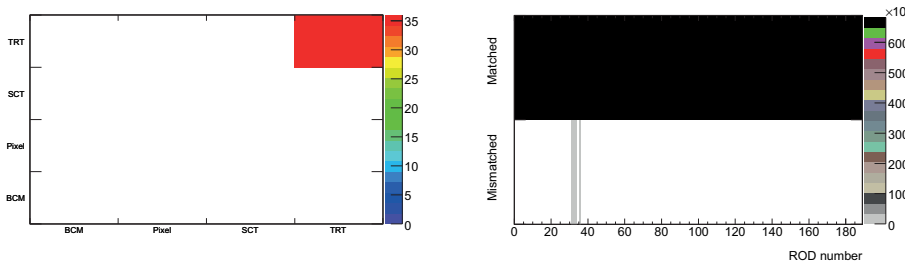

(a) (b)

Figure 5.7: a) An example plot of a warning histogram showing that during 35 events the BCID of some of TRT RODs were mismatched with their neighbor RODs BCIDs. b) An example plot of a clarifying histogram, helping to trace the RODs which were mismatched.

checks on the histograms whenever possible. This check is done in addition to the check performed by a human shifter to provide an initial assessment. The checks can be as simple as to check if the histogram is not empty and as complex as to check if the shape of the distribution is as expected. The results of these checks are combined into DQ flags, provided and stored for each monitoring system. The flags can have five different values: good (green), flawed (yellow), bad (red), undefined (gray) and off (black). The online checks need to be confirmed by the offline event reconstruction, on the one hand to verify the online decision and on the other hand to clarify undefined flags. The final DQ decisions are stored into a database for further analysis. The ID Global monitoring sets one DQ flag which is stored in the database under *IDGL* name. The flag can be set automatically after the online and offline DQ checks and by the offline shifter who can override the automatic decision after more detailed checks of the histograms.

5.4 Summary

When I took the responsibility of the ID Global Monitoring package it had very limited functionalities and was suited to work only in the regime of cosmic muon detection. I improved its code, added several new functionalities and added the possibility to work in the proton-proton collision regime. The long cosmic runs in 2008 and 2009 as well as collision runs at the end of 2009 and in the beginning of 2010 were used to commission the performance of the ID Global Monitoring tool. As a result of the commissioning campaign many histograms were improved and several new histograms were added to the tool, making it more useful for the shifters. The status of the tool described in this thesis is as of the beginning of 2010, when I finished my duties as a developer of the ID Global Monitoring tool. Since then the tool has evolved and some of the descriptions above are not valid anymore.

Chapter 6

Search for New Physics with heavy particles

There are several unsolved mass problems in the present particle physics. The fact that W and Z bosons are heavy while photon is massless is presently explained by Higgs mechanism [6], but the Higgs particle was not observed yet [3] [45]. Precise electroweak measurements point to the Higgs boson being lighter than 148 GeV at 95% C.L [46]. Such a light Higgs boson means that the Standard Model breaks down well before the GUT scale.

Another unsolved problem is large difference between masses of elementary fermions. The top quark, the heaviest elementary particle has the mass close to the electroweak scale. Its influence on the mass of the Higgs boson leads to a conjecture that there exist a scalar version of the top, which partially cancels this influence. In SUSY, one of the theories where such scalar tops exist, the partners of top, bottom and tau can be light due to the mass splitting introduced by the masses of third family fermions. If SUSY exists final states of decay of supersymmetric particles might contain excess of tau leptons, top and bottom quarks compared to what is expected in the SM. Thus production and properties of third family (generation) particles might reveal properties of beyond the SM physics.

The top quark is one of the most powerful tools used both for constraining the Higgs boson mass and for search for New Physics. In the SM, all quarks and leptons couplings to the Higgs boson (Yukawa couplings) are small compared to the top quark coupling. This introduces large difference between the top quark mass and other fermions masses. This also makes the top quark to be the main contributor into the loop corrections of the Higgs mass creating the hierarchy problem mentioned in section 3.1. Thus the value of the top quark mass and its error put constraints on the Higgs boson mass as seen in figure 6.1. Therefore it is important to measure the top quark mass as precisely as possible.

An example of the search for New Physics with top quarks is the search for even heavier particles decaying to the pair of $t\bar{t}$ quarks. For this purpose the cross-section of the $t\bar{t}$ production needs to be estimated and measured accurately. Any excess in the estimated $t\bar{t}$ system invariant mass spectrum can indicate the presence of $t\bar{t}$ resonances predicted by several beyond the Standard Model theories (see section 3.2). The measurement of the electric charge of the top quark can directly indicate the New Physics [47] if the measured value differs from the one, predicted by the SM. The difference between the expected and measured values of the top quark spin polarization and correlations in $t\bar{t}$ events can be a sign of New Physics. In some beyond the Standard

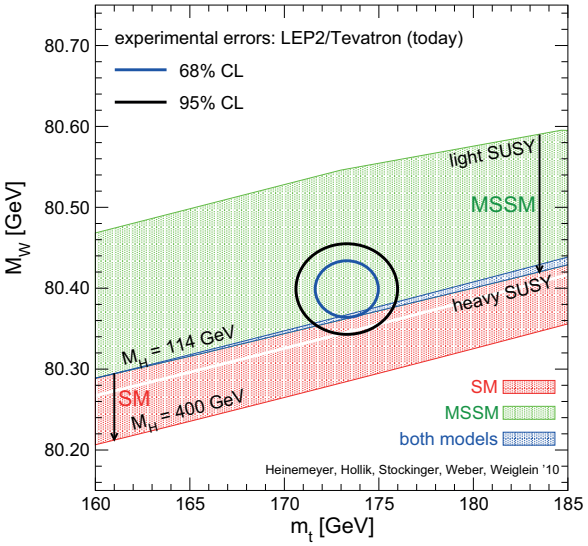

Figure 6.1: Top quark and W boson mass constraints to the Higgs boson mass and SUSY parameters. The allowed region in the MSSM, corresponding to the light-shaded (green) and dark-shaded (blue) bands, results from varying the SUSY parameters independently of each other in a random parameter scan. The allowed region in the SM, corresponding to the medium-shaded (red) and dark-shaded (blue) bands, results from varying the mass of the SM Higgs boson from M_H = 114 GeV to M_H = 400 GeV. (Plot is taken/updated from [4]).

Model theories, the value of the $|V_{tb}|$ element of the Cabibbo–Kobayashi–Maskawa matrix described in chapter 2 can be different than the SM prediction [48], [49]. Some other extensions of the Standard Model predict the Flaviour Changing Neutral Currents (FCNC) at the tree level [50], [51] while the Standard Model allows only small contribution of the FCNC at the loop level [52], [53]. Thus the search for decays of the top quark to another up-type quark and a neutral boson can be used to test the Standard Model and to search for physics beyond it. All above mentioned studies are possible to conduct thanks to the large mass of the top quark and its short life-time making it the only quark which decays before hadronizing.

The heaviest lepton, τ lepton, is also a commonly used tool in the searches for New Physics, especially for SUSY. SUSY models in general violate the $e/\mu/\tau$ universality. In some regions of SUSY parameters (large $tan\beta$) the signatures involving τ leptons become dominant making τ leptons attractive both for search for SUSY particles and for measurements of their properties (mainly masses).

As stated above the measurement of the properties of the top are important in the sense of the search for New Physics. The sensitivity of the ATLAS experiment to the measurement of the top quark properties is evaluated in the paper "Expected performance of the ATLAS experiment: detector, trigger and physics" using Monte Carlo simulations. The top quark charge is one of these properties. The aim of the measurement of the top quark charge is to check if it has the value predicted by the SM (+2/3e) or the particle discovered at Tevatron is not a top quark but an exotic quark with charge $-4/3$e as claimed in Ref. [47]. The measurement of the top quark charge is

carried out by reconstructing the charges of its decay products in the lepton+jets channel of $t\bar{t}$ events. The charge of the W boson is relatively easy to reconstruct since the charged lepton (electron of muon) to which it decays has the same charge as the W boson. The measurement of the charge of the b quark is harder. It is measured by two methods: track charge weighting and semi-leptonic decays of B hadrons. The former one is based on finding a correlation between the b quark charge and the charges of the tracks belonging to the jet it forms (b-jet). In the later method the charge of the b quark is determined via semi-leptonic decays of B hadrons, where the sign of the lepton (decay product of B hadron) can indicate the sing of the b quark charge. Another challenge of the top quark charge measurement is the correct pairing of the lepton and the b quark to ensure that they are decay products of the same (anti-)top quark. This is done using the fact that if they are products of the same (anti-)top quark then their invariant mass can not exceed the top mass (see figure 1 of paper 2), while if they are not correlated then their invariant mass can be both less or more than the top quark mass. The results of the simulations using both methods show that ATLAS is able to distinguish between the SM and exotic scenarios with 0.1-1 fb^{-1} data.

The top quark charge has been measured with proton-proton collision data as soon as enough data (0.7 fb^{-1}) was collected by the ATLAS experiment. The results of this measurement is documented in the paper "Measurement of the top quark charge in pp collisions at $\sqrt{s} = 7$ TeV in the ATLAS experiment". The measurement is done with the techniques described above except that more advanced way of pairing of the lepton and b-jet is used for "semi-leptonic decays of B hadrons" method. The pairing is done using Kinematic Likelihood Fitter to increase the efficiency of the method. The hypothesis that the top quark is instead an exotic quark with charge $-4/3$e is excluded at more than five standard deviations in this paper.

Another simulation based study involving top quarks is documented in paper "On the Possibility of the Search for Top–Antitop Resonances at the LHC". The paper is dedicated to the estimation of the possibility to find generic heavy particles (Z') decaying to $t\bar{t}$ pair at the LHC for $\sqrt{s} = 14$ TeV. The analysis makes use the lepton+jets signature of $t\bar{t}$ events. Five different masses of the resonance are considered: 0.7, 1.0, 1.5, 2.0 and 3.0 TeV. Two types of event selection (loose and tight), three methods of top quark reconstruction (reconstructed mass closest to the generated, highest transverse momentum of top quarks and smallest ΔR between jets) and two ways of Z' reconstruction (with and without cut on the transverse momentum of top quarks) are examined. Tight event selection together with the requirement of the reconstructed top quark mass to be closest to the generated one was selected as the base method. The cut on the transverse momentum of top quarks has shown to improve the resolution and accuracy of the Z' mass measurements. In addition, the case when reconstruction of the final state is done without making use of b-tagging information is also briefly studied. The minimal cross-sections of Z' production needed to discover it are estimated for data corresponding to 1-300 fb^{-1} of integrated luminosity. The analysis is phenomenological and does not consider systematic errors and other backgrounds than direct production of $t\bar{t}$ events.

Among other studies carried out by the ATLAS collaboration using Monte Carlo simulations, the ones dedicated to the measurement of SUSY parameters (mostly particles masses) are documented in paper "Expected performance of the ATLAS experiment: detector, trigger and physics". By measuring the endpoint of the invariant mass

distribution of two charged leptons, final products of SUSY particles decays, it is possible to obtain a relation between masses of lightest neutralino, $\tilde{\chi_1}^0$, next-to-lightest neutralino, $\tilde{\chi}_2^0$, and slepton, $\tilde{\ell}$ with help of the following equation:

$$m_{\ell\ell}^{edge} = m_{\tilde{\chi}_2^0}\sqrt{1-\left(\frac{m_{\tilde{\ell}}}{m_{\tilde{\chi}_2^0}}\right)^2}\sqrt{1-\left(\frac{m_{\tilde{\chi}_1^0}}{m_{\tilde{\ell}}}\right)^2}. \tag{6.1}$$

The endpoint measurement for the cases when leptons are electrons or muons is relatively easy since the invariant mass distribution in these cases has sharp edge which is not the case for tau leptons. Due to the presence of neutrinos from the tau decays, the $m_{\tau\tau}$ distribution (where $m_{\tau\tau}$ indicates the visible decay products of tau pairs) falls off smoothly below the maximum value given by equation 6.1. Despite this, it is still possible to find the endpoint by fitting $m_{\tau\tau}$ distribution with function:

$$f(x) = \frac{p_0}{x}\cdot exp\left(-\frac{1}{2p_2^2}(ln(x)-p_1)^2\right), \tag{6.2}$$

finding the inflection point, m_{IP}, and relating it to the endpoint, m_{EP}, with help of a linear calibration function:

$$m_{IP} = (0.47\pm0.02)m_{EP} + (15\pm2)GeV, \tag{6.3}$$

obtained from Monte Carlo-based calibration procedure. Only hadronic decaying tau leptons could be unambigously identified in the ATLAS setector with help of tau identification algorithms. Two such algorithms are part of the ATLAS reconstruction software. One of them seeds tau candidates from tracks in Inner Detector and searches for energy deposition in the calorimeter while the other first selects a cluster in the calorimeter and then looks if there are tracks behind this cluster. At the time of this study the track-seeded had higher efficiency for low-p_T taus while the calorimeter-seeded was more efficient in high p_T region. The endpoint is determined for two SUSY points: "Coannihilation" and "Bulk". The estimations show that for "Bulk" point the endpoint can be measured already with 1 fb^{-1} of integrated luminosity. Since the cross-section of the "Coannihilation" point is considerably lower more data (up to 18 fb^{-1}) is needed to perform a good fit and estimate the endpoint in this case.

Chapter 7

Concluding remarks and further work

Three different methods of the search for New Physics are presented in the dissertation. One of the searches is performed by measuring the top quark charge from the data of the ATLAS experiment and comparing the results with the hypothesis of the existence of an exotic quark with electric charge of $-4/3e$. As a result of this measurement the hypothesis assuming that the particle with mass $\sim$ 172 GeV observed at the LHC is an exotic quark was ruled out by more than 5 standard deviations. Another analysis involving top quarks estimates the possibility of the LHC experiments to detect extra gauge bosons via their decays to top-antitop pair. This can be done by searching for an excess of events in the top-antitop invariant mass spectrum predicted by the Standard Model. The third analysis is again based on the simulations and checks the possibility of the ATLAS detector to reconstruct the end-point of di-tau invariant mass distribution in the stau co-annihilation region of mSUGRA model. Although the specific models on which the study was performed are already excluded with the ATLAS data, SUSY with taus is still a viable model in the slightly higher mass range. If SUSY with taus is discovered, the techniques to measure $m_{\tau\tau}$ endpoint presented in this thesis can be applied. Several of my colleagues form the University of Bergen are currently analyzing the ATLAS data trying to find an indication of SUSY with tau leptons.

To perform the above mentioned and any other analysis on the ATLAS detector, one first needs to ensure that the detector is working as expected. For this purpose a software intended to monitor the ATLAS Inner Detector was developed and commissioned with cosmic muons and with first data from proton-proton collisions at the LHC. The software is currently running both in online data taking and offline bulk reconstruction modes and its results are used by shifters to monitor the ATLAS Inner Detector.

Searches of heavy $t\bar{t}$ resonances have been performed by the ATLAS collaboration and up to date no evidence of New Physics is observed [54]. The search is performed continuously, and with more data higher masses of particular types of resonances can be excluded and lower limits on the production of generic resonances can be set.

SUSY search is one of the tasks in which many of ATLAS collaboration members are involved. No signal is observed and models with parameters in certain ranges are excluded [55] [56] [57]. The search for SUSY is also a continuous process. The more data ATLAS collects the higher masses of SUSY particles can be possibly discovered. If SUSY is the solution to the hierarchy problem the masses of SUSY particles are kinematically accesible at the LHC. Thus SUSY will be either discovered or excluded by the LHC experiments.

Bibliography

[1] Ugo Amaldi, Wim de Boer, and Hermann Furstenau. Comparison of grand unified theories with electroweak and strong coupling constants measured at LEP. *Phys.Lett.*, B260:447–455, 1991. (document), 3.1

[2] The ATLAS Collaboration, G. Aad et al. Expected Performance of the ATLAS Experiment Detector, Trigger and Physics. *CERN-OPEN-2008-020*, 2008. (document), 4.2, 4.2

[3] The ATLAS Collaboration, G. Aad et al. Update of the Combination of Higgs Boson Searches in pp Collisions at sqrt(s) = 7 TeV with the ATLAS Experiment at the LHC. *ATLAS-CONF-2011-135*, Sep 2011. (document), 4.2, 4.3, 6

[4] Sven Heinemeyer, Wolfgang Hollik, Dominik Stöckinger, Arne M. Weber, and Georg Weiglein. Precise prediction for M_W in the MSSM. *Journal of High Energy Physics*, 2006(08):052, 2006. (document), 6.1

[5] Particle Data Group, K Nakamura et al. Review of Particle Physics. *Journal of Physics G: Nuclear and Particle Physics*, 37(7A):075021 and 2011 partial update for the 2012 edition., 2010. 1, 2, 2.2, 2.1, 4.2

[6] Peter W. Higgs. Broken Symmetries and the Masses of Gauge Bosons. *Phys. Rev. Lett.*, 13:508–509, Oct 1964. 1, 6

[7] Tevatron Electroweak Working Group, CDF and D0 Collaborations. Combination of CDF and D0 results on the mass of the top quark using up to 5.8 fb^{-1} of data. *FERMILAB-TM-2504-E*, Jul 2011. 1

[8] V. Christianto and F. Smarandache. Thirty Unsolved Problems in the Physics of Elementary Particles. *Progress in Physics*, 4:112–114, 2007. 1, 3

[9] F. Zwicky. Die Rotverschiebung von extragalaktischen Nebeln. *Helvetica Physica Acta*, 6:110–127, 1933. 1

[10] F. Zwicky. On the Masses of Nebulae and of Clusters of Nebulae. *Astrophysical Journal*, 86:217, oct 1937. 1

[11] CDF Collaboration, F. Abe et al. Observation of Top Quark Production in $\overline{p}p$ Collisions with the Collider Detector at Fermilab. *Phys. Rev. Lett.*, 74:2626–2631, Apr 1995. 2

[12] D0 Collaboration, S. Abachi et al. Observation of the Top Quark. *Phys. Rev. Lett.*, 74:2632–2637, Apr 1995. 2

[13] The ATLAS Collaboration, G. Aad et al. Measurement of the top quark-pair production cross section with ATLAS in pp collisions at $\sqrt{s} = 7$ TeV. *Eur. Phys. J. C*, 71:1577, 2011. 2

[14] The CMS Collaboration, V. Khachatryan et al. First measurement of the cross section for top-quark pair production in proton–proton collisions at. *Physics Letters B*, 695(5):424 – 443, 2011. 2

[15] M. Jeżabek and J.H. Kühn. QCD corrections to semileptonic decays of heavy quarks. *Nuclear Physics B*, 314(1):1 – 6, 1989. 2

[16] I. Bigi, Y. Dokshitzer, V. Khoze, J. Kühn, and P. Zerwas. Production and decay properties of ultra-heavy quarks. *Physics Letters B*, 181(1-2):157 – 163, 1986. 2

[17] The ATLAS Collaboration, G. Aad et al. Performance of the ATLAS Secondary Vertex b-tagging Algorithm in 7 TeV Collision Data. *ATLAS-CONF-2010-042*, Jul 2010. 2.2

[18] The ATLAS Collaboration, G. Aad et al. Performance of Impact Parameter-Based b-tagging Algorithms with the ATLAS Detector using Proton-Proton Collisions at *sqrts* = 7 TeV. *ATLAS-CONF-2010-091*, Oct 2010. 2.2

[19] The ATLAS Collaboration, G. Aad et al. Reconstruction, Energy Calibration, and Identification of Hadronically Decaying Tau Leptons. *ATLAS-CONF-2011-077*, May 2011. 2.2

[20] Joseph D Lykken. Beyond the Standard Model. *CERN Yellow Report*, pages 101–109, May 2010. 3

[21] Stephen P. Martin. A Supersymmetry Primer. *arXiv:hep-ph/9709356v6*. 3.1, 3.1

[22] Howard Georgi and S. L. Glashow. Unity of All Elementary-Particle Forces. *Phys. Rev. Lett.*, 32:438–441, Feb 1974. 3.1

[23] H. Georgi, H. R. Quinn, and S. Weinberg. Hierarchy of Interactions in Unified Gauge Theories. *Phys. Rev. Lett.*, 33:451–454, Aug 1974. 3.1

[24] H.P. and Nilles. Supersymmetry, supergravity and particle physics. *Physics Reports*, 110(1-2):1 – 162, 1984. 3.1

[25] Christopher T. and Hill. Topcolor assisted technicolor. *Physics Letters B*, 345(4):483 – 489, 1995. 3.2

[26] Nima Arkani–Hamed, Savas Dimopoulos, and Gia Dvali. The hierarchy problem and new dimensions at a millimeter. *Physics Letters B*, 429(3-4):263 – 272, 1998. 3.2

[27] Nima Arkani-Hamed, Savas Dimopoulos, and Gia Dvali. Phenomenology, astrophysics, and cosmology of theories with submillimeter dimensions and TeV scale quantum gravity. *Phys. Rev. D*, 59:086004, Mar 1999. 3.2

[28] Lisa Randall and Raman Sundrum. Large Mass Hierarchy from a Small Extra Dimension. *Phys. Rev. Lett.*, 83:3370–3373, Oct 1999. 3.2

[29] Lisa Randall and Raman Sundrum. An Alternative to Compactification. *Phys. Rev. Lett.*, 83:4690–4693, Dec 1999. 3.2

[30] Oliver Sim Brüning, Paul Collier, P Lebrun, Stephen Myers, Ranko Ostojic, John Poole, and Paul Proudlock. *LHC Design Report*. CERN, Geneva, 2004. 4.1

[31] P Lebrun. Large Cryogenic Helium Refrigeration System for the LHC. *LHC-Project-Report-629*, Feb 2003. 4.1

[32] The ATLAS Collaboration, G. Aad et al. *ATLAS detector and physics performance: Technical Design Report*. Technical Design Report ATLAS. CERN, Geneva, 1999. 4.2

[33] The ATLAS Collaboration, G. Aad et al. The ATLAS Experiment at the CERN Large Hadron Collider. *Journal of Instrumentation*, 3(08):S08003, 2008. 4.3, 4.4, 4.1

[34] The ATLAS Collaboration, G. Aad et al. The ATLAS Inner Detector commissioning and calibration. *Eur. Phys. J. C*, 70:787–821, Jun 2010. 4.4

[35] The ATLAS Collaboration, G. Aad et al. Estimating Track Momentum Resolution in Minimum Bias Events using Simulation and Ks in sqrt(s) = 900 GeV collision data. *ATLAS-CONF-2010-009*, Jun 2010. 4.4

[36] The ATLAS Collaboration, G. Aad et al. Tracking Results and Comparison to Monte Carlo simulation at sqrt(s) = 900 GeV. *ATLAS-CONF-2010-011*, Jul 2010. 4.4

[37] Performance of the ATLAS Silicon Pattern Recognition Algorithm in Data and Simulation at sqrt(s) = 7 TeV. *ATLAS-CONF-2010-072*, Jul 2010. 4.4

[38] The ATLAS Collaboration, G. Aad et al. The ATLAS Transition Radiation Tracker (TRT) proportional drift tube: design and performance. *Journal of Instrumentation*, 3(02):P02013, 2008. 4.4.3

[39] Rene Brun and Fons Rademakers. ROOT - An object oriented data analysis framework. *Nucl. Inst. and Meth. in Phys. Res*, 389(1-2):81–86, 1997. 4.9, 5.1

[40] T. Sjostrand and S. Mrenna and P.Z. Skands. PYTHIA 6.4 Physics and Manual. *JHEP*, 05:026, 2006. 4.9

[41] G. Corcella et al. HERWIG 6: An Event generator for hadron emission reactions with interfering gluons (including supersymmetric processes). *JHEP*, 0101:010, 2001. 4.9

[42] S. Agostinelli et al. GEANT4 - A Simulation Toolkit. *Nucl. Instr. and Meth.*, A506:250, 2003. 4.9

[43] The ATLAS Collaboration, G. Aad et al. *Atlas Computing: technical design report*. CERN, Geneva, 2005. 4.9

[44] S Kolos, A Corso-Radu, H Hadavand, M Hauschild, and R Kehoe. A software framework for Data Quality Monitoring in ATLAS. *J. Phys.: Conf. Ser.*, 119:022033, 2008. 5.3

[45] CMS Collaboration. Combination of Higgs Searches. *CMS-PAS-HIG-11-022*, 2011. 6

[46] Jens Erler. Mass of the Higgs boson in the standard electroweak model. *Phys. Rev. D*, 81:051301, Mar 2010. 6

[47] Darwin Chang, We-Fu Chang, and Ernest Ma. Alternative interpretation of the Fermilab Tevatron top events. *Phys. Rev. D*, 59:091503, Apr 1999. 6

[48] J.A. Aguilar-Saavedra. Hierarchy plus anarchy in quark masses and mixings. *Phys.Rev.*, D67:073026, 2003. 6

[49] Francisco del Aguila and Jose Santiago. Signals from extra dimensions decoupled from the compactification scale. *Journal of High Energy Physics*, 2002(03):010, 2002. 6

[50] G. M. de Divitiis, R. Petronzio, and L. Silvestrini. Flavour changing top decays in supersymmetric extensions of the standard model. *Nuclear Physics B*, 504:45, 1997. 6

[51] David Atwood, Laura Reina, and Amarjit Soni. Probing flavor changing top-charm-scalar interactions in $e\hat{+}e\hat{-}$ collisions. *Phys. Rev. D*, 53:1199, 1996. 6

[52] B. Grzadkowski, J.F. Gunion, and P. Krawczyk. Neutral current flavor changing decays for the Z boson and the top quark in two-Higgs doublet models. *Physics Letters B*, 268(1):106 – 111, 1991. 6

[53] G. Eilam, J. L. Hewett, and A. Soni. Rare decays of the top quark in the standard and two-Higgs-doublet models. *Phys. Rev. D*, 44:1473–1484, Sep 1991. 6

[54] The ATLAS Collaboration, G. Aad et al. A Search for ttbar Resonances in the Dilepton Channel in 1.04 fb^{-1} of pp Collisions at sqrt(s) = 7 TeV. *ATLAS-CONF-2011-123*, Aug 2011. 7

[55] The ATLAS Collaboration, G. Aad et al. Searches for supersymmetry with the ATLAS detector using final states with two leptons and missing transverse momentum in *sqrts* = 7 TeV proton-proton collisions. *arXiv:1110.6189v1 [hep-ex]*, 2011. 7

[56] The ATLAS Collaboration, G. Aad et al. Search for supersymmetry in final states with jets, missing transverse momentum and one isolated lepton in $\sqrt{s} = 7$ TeV pp collisions using 1 fb-1 of ATLAS data. *arXiv:1109.6606v1 [hep-ex]*, September 2011. 7

[57] CMS Collaboration. Search for Supersymmetry at the LHC in Events with Jets and Missing Transverse Energy. *arXiv:1109.2352v1 [hep-ex]*, September 2011. 7